DESIGN AND OPERATION OF MEMBRANE MICROCALORIMETERS FOR THERMAL SCREENING OF HIGHLY ENERGETIC MATERIALS

A Dissertation

by

VICTOR HUGO CARRETO VAZQUEZ

Submitted to the Office of Graduate Studies of
Texas A&M University
in partial fulfillment of the requirements for the degree of

DOCTOR OF PHILOSOPHY

December 2010

Major Subject: Chemical Engineering

DESIGN AND OPERATION OF MEMBRANE MICROCALORIMETERS FOR THERMAL SCREENING OF HIGHLY ENERGETIC MATERIALS

A Dissertation

by

VICTOR HUGO CARRETO VAZQUEZ

Submitted to the Office of Graduate Studies of
Texas A&M University
in partial fulfillment of the requirements for the degree of

DOCTOR OF PHILOSOPHY

Approved by:

Co-Chairs of Committee,	Sam M. Mannan
	Dragomir B. Bukur
Committee Members,	Victor M. Ugaz
	Cesar O. Malavé
Head of Department,	Michael Pishko

December 2010

Major Subject: Chemical Engineering

ABSTRACT

Design and Operation of Membrane Microcalorimeters for Thermal Screening of Highly Energetic Materials. (December 2010)

Víctor Hugo Carreto Vazquez, B.S., Instituto Politécnico Nacional;

M.S., Texas A&M University

Co-Chairs of Advisory Committee: Dr. Mahboobul S. Mannan
Dr. Dragomir B. Bukur

Following several terrorist attacks that have occurred during this decade, there is an urgent need to develop new technologies for the detection of highly energetic materials that can represent an explosive hazard. In an effort to contribute to the development of these new technologies, this work presents the design aspects of a chip-scale calorimeter that can be used to detect an explosive material by calorimetric methods. The aim of this work is to apply what has been done in the area of chip-scale calorimetry to the screening of highly energetic materials. The prototypes presented here were designed using computer assisted design and finite element analysis tools. The design parameters were set to satisfy the requirements of a sensor that can be integrated into a portable system (handheld) for field applications. The design approach consisted of developing a sensor with thick silicon membranes that can hold micro-size samples and that can operate at high temperatures, while keeping the cost of the sensor low. Contrary to other high resolution systems

based on thin-film membranes, our prototypes exhibit a contribution from addenda that is comparable to that from the sample, and hence they have lower sensitivity. However, using thick membranes offers the advantage of producing sensors strong enough for this application and that have significantly lower cost. Once the prototypes were designed, the fabrication was performed using standard microfabrication techniques. Finally, the operation of our prototypes was demonstrated by conducting thermal analysis of different liquid and solid samples.

DEDICATION

I dedicate this work to my beloved family (Ivonee, Axayácatl, and Itzel) for all their love and support. Also, I thank all my family in México for all they have done for me. Their love sustained me through these years away from my home town.

I really thank God for giving me the opportunity to know so many wonderful people. I dedicate this work to Him because without His blessing nothing is possible.

ACKNOWLEDGEMENTS

I would like to thank my committee chairs, Dr. Mannan and Dr. Bukur, and my committee members, Dr. Ugaz and Dr. Malavé, for their guidance and support throughout this research. I gratefully thank Dr. Liu for her contribution to this work.

Thanks also go to my dear friends and colleagues and the department faculty and staff for making my time at the Mary Kay O'Connor Process Safety Center a great experience. Special thanks to Valerie, Donna, Mary, Towanna, and Randy, for making my life easier at the Chemical Engineering Department.

I would like to thank Mr. Mike O'Connor because his vision made possible the existence of the Center. Thanks to the Steering and the Technical Advisory Committee members for their valuable guidance. My special thanks to Dr. Kletz, Dr. Pasman, Dr. Papadaki, Dr. Vazquez, Dr. Mashuga, and Mr. Johnstone for generously sharing their enormous knowledge and experiences.

I also want to extend my gratitude to the National Council on Science and Technology (CONACyT) for its financial support during this time at Texas A&M University. Thanks to all the people that helped me and supported me in any or other way.

NOMENCLATURE

DAQ	Data acquisition system
DC	Direct current
DSC	Differential scanning calorimetry
DTA	Differential thermal analyzer
HEM	Highly energetic material
HMTD	Hexamethylene triperoxide diamine
MEMS	Microelectromechanical systems
PCB	Printed circuit board
PEEK	Polyether ether ketone
RIE	Reactive ion etching
RTD	Resistance temperature detector
TATP	Triacetone triperoxide
TNT	Tinitro toluene
A	Cross sectional area of the heater
Cp	Specific heat capacity at constant pressure, J/kg-K
E	Thermal radiation constant
I	Current flowing through the resistive heater, amps
J	Input current density, amps/m^3
L	Length of the heater, m
Q	Heat sources other than viscous heating, W/m^3

Q_{Joule}	Joule heating, W
R(T)	Resistance as function of temperature, ohms
S_{heater}	Surface area of the heater, m^2
S_{RTD}	sensor output
T_{amb}	Ambient temperature, K
T_e	External temperature, K
T_o	Reference temperature, K
$T_{surface}$	Surface temperature, K
k	Material thermal conductivity, W/m-K
n	Normal vector of the lateral walls
q_{joule}	Joule heating per unit area, W/m^2
q_o	Inward heat flux, which is normal to the boundary, W/m^2
u	Velocity vector, m/s
α	Temperature coefficient of resistivity, $\%/^oC$
δ_o	Resistivity at the reference temperature, ohm-m
ρ	Material density, kg/m^3

TABLE OF CONTENTS

Page

Page

LIST OF FIGURES

Page

Page

Page

LIST OF TABLES

Page

1. INTRODUCTION

Calorimetry is a useful tool in chemical engineering because it provides a simple and universal method for characterizing materials and processes [1]. It has multiple applications including material properties characterization, chemical kinetics research, and the assessment of reactive chemicals hazards [2-6]. There are different calorimetric techniques, including differential scanning calorimetry (DSC), reaction calorimetry, and adiabatic calorimetry. Among these three types of calorimetric techniques, the simplest and most commonly used is DSC. This technique offers fundamental information including heat of transition, mixing, decomposition, or reaction, which can be studied in detail through calorimetric measurements. Unfortunately, conventional DSC techniques are difficult to use in applications where the samples are very small because the sensitivity required is very high [7].

Evolving areas of research and new applications where thermal analysis of small samples is required has increased the interest for investigating and developing new calorimetric tools. For example, the use of chip-scale calorimeters based on micro electro mechanical systems (MEMS) has been in constant development for the last twenty years. These new calorimeters bring in the possibility of creating small devices of relatively low cost that potentially can translate the analysis from the laboratory to the field by using handheld

---

This dissertation follows the style of *Journal of Hazardous Materials*.

calorimeters. However, this requires refinements to the technique and the development of new devices that currently are not commercially available.

In this dissertation, I will first present background information about the research that other groups have done using chip-scale calorimeters. Following this introduction, I will describe a new application for these devices that our research group is developing. Then, I will detail the various tools and methods used to conduct this research on the design of a chip-scale calorimeter for screening of highly energetic materials. Finally, I will proceed to discuss the results obtained in this work, propose possible future work, and conclude with a short summary.

1.1 MEMS-based calorimeters

Multiple peer-review papers have reported the design and use of miniaturized calorimeter systems [8]. One major challenge in developing these devices arises from the fact that thermal signals from small samples are also small and difficult to measure. These calorimeters were optimized for measuring small amounts of energy in the order of few micro joules and even nano joules for very sensitive devices [9-18]. Such high sensitivities have allowed the investigation of thermal transitions of nanomaterials [19-22], biological systems [23-29], polymers [19-20, 30-31], sensing of combustible gases [32-33], among other applications where high sensitivity is required. With the intent of reaching

such high sensitivities, nano- and microscale calorimeters have been fabricated on thin membranes of silicon nitride suspended on silicon frames. The design approach employed in their fabrication is to create very thin membranes with very small thermal mass, which is translated into devices with high sensitivity and ultrafast response times [34].

Despite the multiple applications where these devices have shown an excellent performance, none of these devices has been optimized for field applications or for thermal screening of highly energetic materials (hereafter referred as HEM). The reduced thickness of their membrane makes them extremely fragile and requires delicate operation to place the sample. Additionally, with the exception of the devices manufactured by Xensor Integration [35], most of these calorimeters were tailored for a specific application and they are not commercially available.

1.2 Energetic materials and terrorist threats

Chemical nature of some substances makes them very sensitive or unstable and in cases when their energy content is high, these materials may represent a significant hazard if not handled properly. For example, in the case of organic peroxides under the right conditions, these compounds can liberate enough energy to be a hazard. Some organic peroxides are shock-sensitive and explosive, others are more stable, but contamination makes them more

sensitive. Energy content of organic peroxides may not be of the same magnitude as for high explosives. However, their value to terrorists is not their performance, it is the simplicity for their preparation and easy access [36], and because they are more difficult to detect using current technologies.

1.3 Use of calorimetry for explosive detection

The idea of using calorimetry as a tool for detection of HEM has been explored by different research groups [1, 37-40]. In 2002, Bannister et al. first proposed the application of calorimetry for detection of energetic materials in samples of unknown composition. In the US patent No. 6,406,918 B1, the authors emphasized the advantages of using calorimetry for explosive detection over traditional detection techniques [38]. Because an explosive can be prepared from different types of materials, it is very difficult that a single traditional detection system can detect all types of explosives, which results in possible false negatives during the screening process. However, detectors based on calorimetric sensors offer an alternative way of overcoming these problems. The concept behind the use of calorimeters as explosive detectors is relatively straightforward. A thermal screening of an unknown sample may be used to determine the existence of an exothermic behavior. The relative thermal hazard of an unknown sample can be evaluated from information obtained from a thermal scan, which includes the position of the exotherms, and its relative intensity and energy content. Sharp exotherms with relatively high area under

the peak, will be a sign of the possible presence of a HEM ($i.e.$, explosives). On the other hand, insignificant exothermic behavior or its complete absence can be used to designate a material as not hazardous from the point of view of thermal energy content. An advantage of this approach is that this method can be used to screen materials for the presence of explosives regardless of their composition. Therefore, they can be used to detect any kind of explosives and help reduce the number of false negatives [1, 37].

1.4 Limitations of traditional calorimetry for screening of HEM

Typical calorimeters used for reactive chemical research require relatively large amounts of sample ($i.e.$, few grams) for obtaining reliable results. This feature in fact limits their use for analysis of HEM because the high energy content of these substances increases the chances of damaging the equipment during the tests [41]. Even differential scanning calorimeters (DSC's) and differential thermal analyzers (DTA's), which require small amounts of sample ($i.e.$, few milligrams) have this limitation. It is possible to reduce the sample size but the sensitivity of the apparatus has to be very high to obtain meaningful results. As an alternative, the use of MEMS-based techniques provides an effective way to fabricate highly sensitive calorimeters that can use very small samples in order to overcome the limitations of traditional calorimeters for screening of highly energetic materials.

It is important to understand that variations in the composition or concentration of the samples screened using chip-scale calorimeters will affect the position and intensity of the peaks in the same way that they affect traditional differential scanning calorimeters [42]. Therefore, identification of the specific substance by thermal screening may result in a nontrivial task, and thermal screening cannot be considered as a stand-alone technique for the identification of energetic substances for security applications. However, quick measurements of the potential exothermic behaviors will be an excellent determining factor of conducting further testing to identify an unknown sample.

2. MOTIVATION AND PROBLEM STATEMENT

2.1 Motivation

Almost all the current explosive detection techniques developed until now focus on identifying common nitrogen-based military explosives. However, as the access to traditional explosives becomes more controlled and restricted, it is likely that terrorists will try to use different materials for their attacks. For example, it has been reported that peroxides with multiple –O–O– functionalities per molecule including TATP (triacetone triperoxide) and HMTD (hexamethylene triperoxide diamine) can have TNT equivalences of around 88% and 60%, respectively [36]. These compounds can easily be transported hidden in the luggage or disguised as other materials. In the case of TATP, it is a very powerful explosive that unlike many conventional explosives, do not contain nitro- groups, which makes its detection by traditional detection systems quite difficult. TATP has an inoffensive appearance similar to sugar. However, as mentioned above its power is close to TNT. The value of TATP and other HEM for the terrorist is the ease with which materials required for their synthesis can be obtained [43-44]. In addition, the mobility of terrorists makes possible that they try to target practically any location and not only secured facilities such as airports and government offices. As happened in the London bombings in 2005, where several people died or received injuries as a result of terrorist attacks using TATP [45].

2.2 Problem statement

As mentioned above, non-conventional explosives are difficult to detect with current technologies. The explosion potential of substances can, however, be estimated from their thermal analysis. This type of analysis can determine the explosive tendency of an unknown sample based on the energy content obtained from thermal analysis. Unfortunately, due to limitations associated with their size, cost, and throughput, there are not commercially available calorimeters that are suitable for deployment to detect explosives in field applications. In addition, the use of calorimeters for the thermal characterization of explosive materials has been limited because energetic materials can contain enough explosive power to damage the equipment during the test. With all this in mind our ultimate goal is to contribute to the development of a detection tool that is able to detect HEM regardless of their composition, and that can be easily deployed where needed. We proposed the use of chip-scale calorimeters to determine if a solid or liquid sample is a threat or not.

3. CALORIMETER DESIGN

The approach for the calorimeters design consisted of using computer assisted design (CAD) and finite element software tools for defining preliminary prototypes and estimating their performance before proceeding to fabrication (Figure 1). This approach was chosen to reduce the cost associated with the fabrication of the device and to explore the effect of the variables that affect the design including geometries of heaters, location of heaters and temperature sensors, materials of construction and metal layer thickness. These factors will be discussed in more detail later in this manuscript.

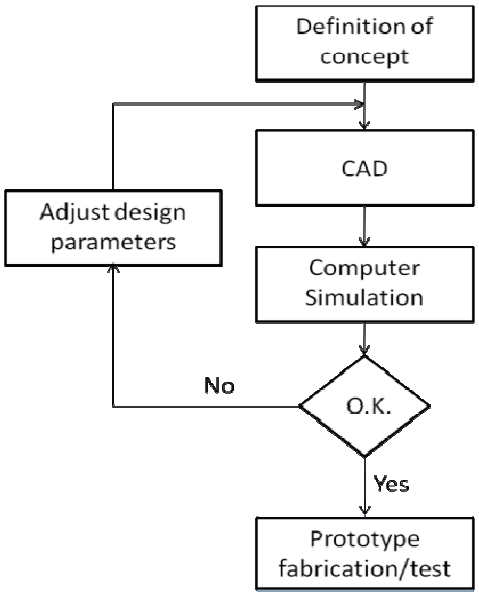

Figure 1 Schematics of the design approach used in this work.

3.1 Definition of concept

The application of chip-scale calorimeters for screening of HEM requires that the device fulfills a number of requirements, which include general and specific requirements. The former ones related to the whole apparatus, and the latter ones related to the calorimeter sensor itself. General requirements include portability, simple operation, easy results interpretation, and low acquisition and operation cost. All these factors are related to the hardware and electronics and won't be discussed here. On the other hand, specific requirements define the design of the calorimeter sensor for studying the thermal behavior of HEM. These include broad operating temperature range, high sensitivity, and low power consumption.

Operating temperatures – The desired operating temperature range of the calorimeter sensor was fixed by the expected temperature at which an exothermic behavior can be detected for an explosive material. For this work, the exothermic behavior is associated with combustion, intense decomposition or detonation of the sample, and hereafter will be simply referred to as sample decomposition. As it can be observed in Table 1, common explosives have thermal decompositions in the range of 250-380^{o}C. Therefore, the calorimeter sensor should be designed to work in this temperature range.

Table 1 Heat of decomposition and melting and decomposition temperatures for some common explosive materials (extracted from [46] and [47]).

Name	T_m °C	T_d °C	ΔH decomposition	
			J/g	cal/g
Nitromethane	-29.0	101	4,301	1,028
Trinitro-2,4,6-phenilmethylnitramine (Tetryl)	129.5	185	4,770	1,140
Hexamethylenetriperoxide Diamine (HMTD)	---	200	3,188	762
Dipentaerylthritol Hexanitrate	72.0	200	5,142	1,229
Pentaerylthritol Tetranitrate (PETN)	141.3	205	6,276	1,500
Ammonium Nitrate (AN)	169.6	210	2,630	629
1,3,5,-Trinitro-1,3,5,-triazacyclohexane (RDX)	202	229	5,540	1,324
Ethylene Glycol Dinitrate (EGDN)	---	240	7,130	1,704
1,3,5,7-Tetranitro-1,3,5,7-tetrazacyclooctane (HMX)	276	276	5,669	1,355
Picric Acid	122.5	300	3,351	801
2,4,6-Trinitrotoluene (TNT)	80.7	300	4,230	1,011
Ammonium Picrate	280.0	320	2,870	686
Dinitrotoluene 2,4- isomer(DNT)	70.5	360	3,192	763
Tetranitrodibenzo-1,3 a, 4,6 a-tetrazapentalene (TACOT)	378.0	378	4,100	980
Nitroglycerin (NG)	13.2	4,250	6,276	1,500
Ammonium Perchlorate (APC)‡	---	---	1,971	471

‡: Decomposes on heating

Device sensitivity – The calorimeter sensor was designed to use microgram powder samples. This sample size was set to allow a relatively uncomplicated handling of the samples without requiring special tools and to facilitate operation of the device. In addition, using relatively large samples in comparison to other nanocalorimeter systems reported in the literature, allow designing a system with intermediate sensitivity, which can yet provide useful data for this application with HEM. Also, the reduction in the required sensitivity of the proposed devices simplifies the fabrication process, which keeps the cost sensors of the sensors low for better commercialization. In Table 1 it can be observed that most common explosives have heats of decomposition in the range of 500 cal/g (2,100 J/g) to 2,000 cal/g (8,500 J/g). It has been reported that HEM samples with heat of explosion smaller than 800 cal/g (3,350 J/g) usually do not explode [46]. However, the device should be designed to detect energy amounts below 500 cal/g using micro samples. Therefore, the geometry of the calorimeter sensor and the thickness of the sensing area were defined to allow sensitivity in the millijoule range.

Power consumption – The energy required to operate the calorimeter device will be supplied through an electrical DC power supply. The total electrical power required is defined by the desired maximum temperature range, heating rate, heat losses, and the *addenda* of the device, which is defined by the size of the calorimeter and the thickness of its sensing area. Addenda is defined

as the heat capacity of the calorimeter components and surrounding elements [48].

3.2 Prototype geometry modeling using CAD

The design concept for the calorimeter defined in Section 3.1 was used to generate prototypes using CoventorWare DESIGNER®. This software makes 3D solid models that can be processed later using finite element analysis in COMSOL Multiphysics™ from 2D layouts by virtually resembling the actual micro fabrication process such as metal evaporation, anisotropic wet etching, deep reactive ion etching, etc. Under this approach, it is possible to evaluate several alternative options before a decision is made to construct a calorimeter prototype. The following sections describe in detail the main parameters considered during the design of the calorimeter. For simple explanation, these sections will refer to two of the calorimeter prototypes used in this work, which are described below.

Prototype TAMU/ULL–03: The device prototype shown in Figure 2 has two resistive temperature detectors (RTD). One located on the center of the heated area of the membrane and the other on the silicon frame. This prototype has one resistive heater for normal operation and other for calibration purposes with a resistance of 1-1.2 and 0.6-0.7 kohm, respectively. The calorimeter prototypes have membranes of 50 μm and 10 μm (hereafter referred to as TAMU/ULL-03a

and -03b). The silicon area surrounding the membrane facilitates a good thermal contact between the sensor and the heat sink where the sensor is connected, and provides an area to build the contact pads of the calorimeter. Despite these advantages having a relatively large silicon frame has a detrimental effect on the cost of the devise. Therefore, a final device should have a reduced silicon frame to maximize the number of sensors per wafer.

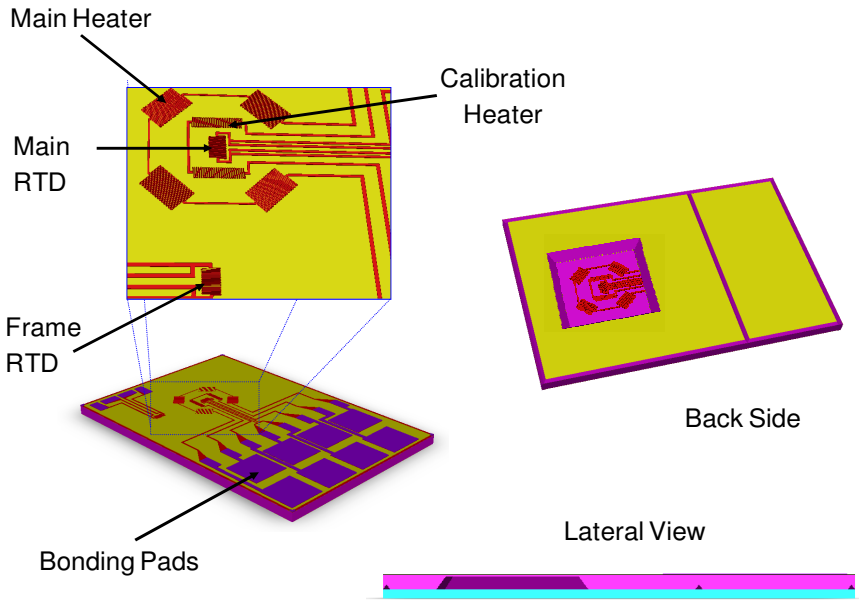

Figure 2 Membrane calorimeter with resistive heaters and RTD sensors fabricated at TAMU/ULL (TAMU/ULL-03).

Prototype TAMU/ULL–04: A second prototype has two membranes with a thin-film resistor of 60-100 ohms on each one. These membranes are separated from each other by a third membrane, which is intended for improving their thermal isolation (Figure 3). In this prototype, the thin-film resistors are used as heaters and temperature sensors simultaneously. The design of the sensor allows placing the reference and the sample cells in a single chip.

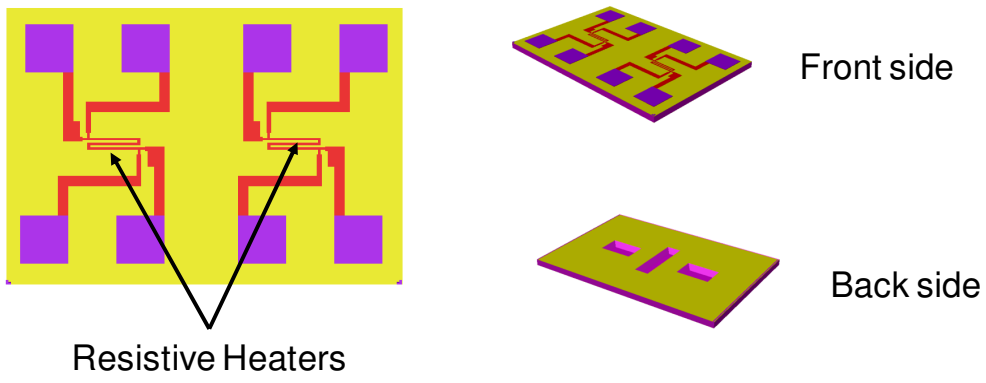

Figure 3 Dual calorimeter fabricated at TAMU/ULL (TAMU/ULL-04).

3.3 Computer simulation using finite element analysis

The aim of using Finite Element Analysis (FEA) tools for the design of the calorimeter is to obtain information about the expected heat transfer in the prototypes and the performance of their resistive heaters and RTDs prior to their fabrication. COMSOL Multiphysics™ (formerly FEMLAB) can be used to construct very detailed models that represent the real geometry. By doing this, a

detailed thermal design that takes into account the addenda of the device, the potential heat losses, and the effect of the geometric parameters is possible.

The process starts by constructing a geometric model of the prototype using CoventorWare™. Then, the geometry is meshed and the appropriate equations that describe the heat transfer and electrical domains are selected. Next is to define the materials properties for each sub-domain in the geometry. After the problem is formulated, the model is run and the design parameters are adjusted for model refinement. The appendix of this dissertation describes in detail the process followed to construct the model for two commercial nanocalorimeters, which are representative examples of one thin-film silicon membrane calorimeter and one calorimeter based on a thick silicon membrane. In the following section, the information obtained from the models is described.

3.3.1 Calorimeter substrate selection

The material for the calorimeter substrate is silicon. This material was selected based on their compatibility with standard micro fabrication techniques. The use of silicon is expected to reduce the calorimeter sensitivity due to its high thermal conductivity [25]. However, from the practical point of view silicon is still the best option for these devices. The silicon substrates were covered with a layer of silicon nitride on both sides to be able to fabricate the membranes by wet etching. An intermediate layer of silicon oxide was added to the electronics

side of the wafer to act as an electrical insulator for the electronics side of the sensor, which prevents temperature sensor shunting at high operating temperatures because of changes in silicon conductivity [49]. Modeling results showed that the thermal resistance of thin-film silicon membranes are close to 50kK/W and for the calorimeters fabricated using thick membranes the thermal resistance is typically reduced to 50-200 K/W depending on the specific design. These values give an idea about the differences in sensitivity of these different types of calorimeters.

3.3.2 Thin-film resistive heaters

The heat required to operate the calorimeters is produced in thin-film resistive heaters when an electrical current flows through them. A thin-film resistor consists of a resistive material layout deposited on the surface of an isolating substrate [50]. The power dissipated by the heaters in the calorimeter is given by Joule's law according to the following expression [51].

$$\boldsymbol{P_d = I^2 \times R} \tag{3.1}$$

where, P_d is the power dissipated by the heater (Watts), I is the steady-state current (Ampere), and R is the steady state resistance (ohm).

Material selection - The prospective materials for the heaters fabrication are selected based on their compatibility with standard metal deposition techniques, their effect on the device performance, linear temperature dependency on the range of interest, and economical reasons. For the heaters/RTDs fabrication, materials with high temperature resistance coefficients (TCR) and low specific resistivity are desired from the point of view of the device sensitivity [49]. For this work, aluminum, gold, and platinum, which meet these criteria, were considered for the design of the calorimeter sensor (see Table 2).

Table 2 Selected properties at room temperature for Al, Au and Pt (extracted from [49]).

Metal	**k** W/m-^{o}C	**Density** kg/m^{3}	**C_P** J/kg-^{o}C	**ρ_o** Ohm-m	**TCR** 1/^{o}C	**T_m** ^{o}C
Al	237	2,700	904	2.82 x10^{-8}	0.00398	660
Au	317	19,300	129	2.44 x10^{-8}	0.0034	1063
Pt	72	21,450	133	1.05 x10^{-7}	0.00392	1770

The plots shown in Figure 4 were obtained to compare the effect of different metallization materials on the performance of the heater. These plots were constructed using a model with constant geometry parameters for the heater ($i.e.$, prototype TAMU/ULL-04a), and different construction materials. As it can be observed, Al, Au, and Pt all exhibit a linear behavior of the resistance as a function of temperature and hence they are suitable for the heaters

fabrication. Each point shown in Figure 4 was obtained by modeling steady-state conditions using a constant power. Maintaining the geometric parameters constant shows that heater fabricated on Pt will exhibit a larger temperature increase. Also, as it can be observed, there is no significant difference between heaters modeled using Au properties and the ones using Al. Therefore, for this work, Al was preferred because it has reduced chemical activity compared to Au and Pt, high adhesion on the substrate materials without requiring adhesion underlayer[49], its availability, and because its cost is the lowest among these three options.

Dimensions and configuration – The dimensions of the heaters define their nominal resistance at room temperature and the power dissipation at a given current flow. The resistance at room temperature of the heaters in the calorimeter is dependent on their geometric parameters (length, width and thickness) and the material selected for their fabrication. This nominal resistance is expressed by:

$$\boldsymbol{R_o = \rho_o \frac{l}{A_c} = \rho_o \frac{l}{w \times t}} \tag{3.2}$$

where, ρ_o is the material bulk resistivity per unit length at room temperature (ohm-m); A_c is the cross sectional area of the heaters (m^2); and l, w, and t are

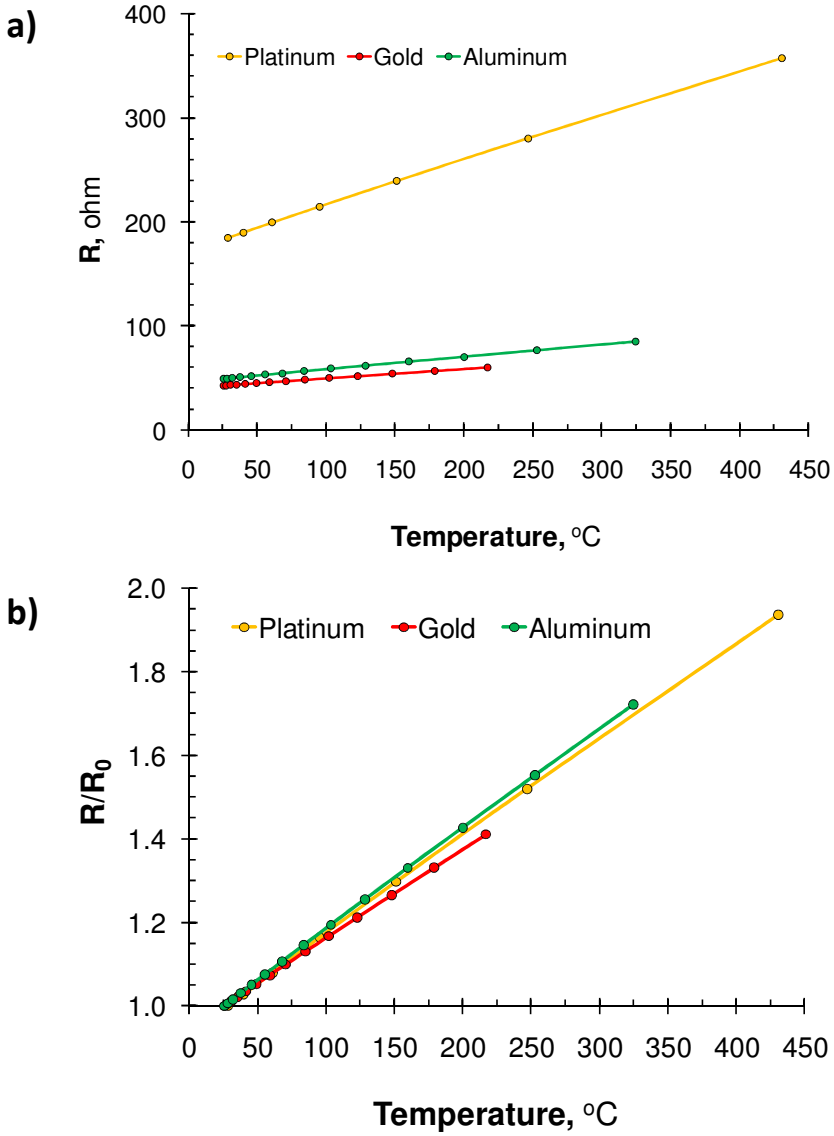

Figure 4 Estimated resistance changes as a function of temperature and heater material. Results were obtained for model prototype TAMU/ULL-04a.

their length (m), width (m), and thickness, respectively. As the material properties, and the length and width of the heaters are initially defined for the prototypes shown in this work, the resistance is now only defined by the thickness of the metallization layer. As it can be observed in Figure 5, which was obtained for prototype TAMU/ULL-03, the dependence of the resistance on the metal thickness is more obvious for layers below 50 μm. Therefore, for our prototypes the controlled metal thickness was maintained above 100 μm. This is because variations during the metal deposition process can lead to significant differences in the metal thickness and the desired nominal resistance of the resistive elements.

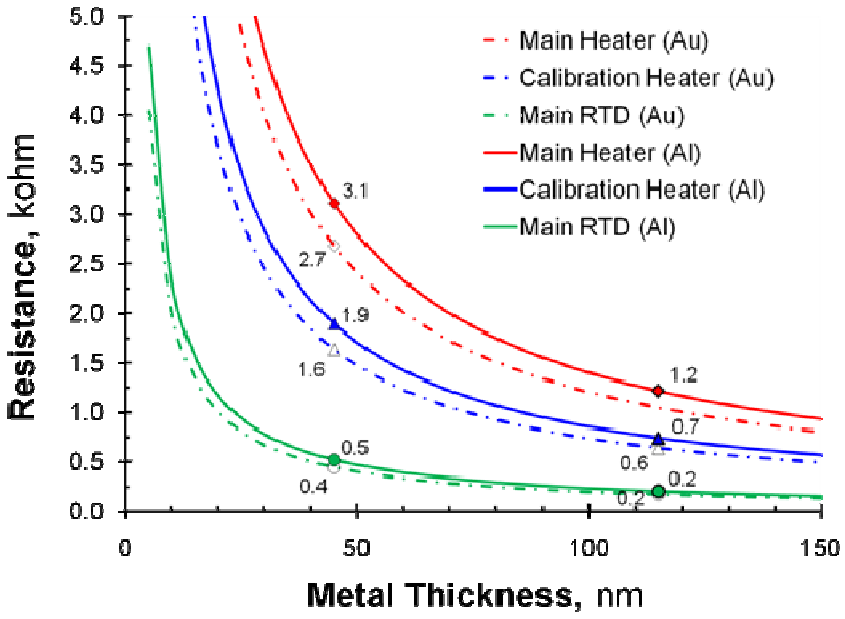

Figure 5 Dependency of resistance of heaters and RTD elements on the metallization layer thickness for prototype TAMU/ULL-03.

On the other hand, the temperature distribution on the calorimeter surface is strongly influenced by the configuration or shape of the heaters and their location. These factors were investigated using 2D and 3D FEA models. The models were built based on general recommendations for the construction of thin-film heaters to limit the number of possible designs. This includes maintaining a large aspect ratio (l/w) to reduce the signal-to-noise ratio (SNR) of the device, and maintaining a heater layout that reduces the thermal gradients across the membrane. The design constraints were the planar dimensions of the membrane, and the desired nominal resistance of the thin-film sensors at room temperature ($R_{o\ RTD}$). The resistors have a meander shape to fit the length of the resistive element within the constraints of the membrane dimensions (see Figure 6). The dimensions of the heaters in prototype TAMU/ULL-03 were adjusted to give a nominal resistance value of 1,000-1,200 and 600-700 ohms for the main and calibration heaters, respectively. In the case of prototype TAMU/ULL-03 the dimensions were adjusted to give a nominal resistance of 60-100 ohms.

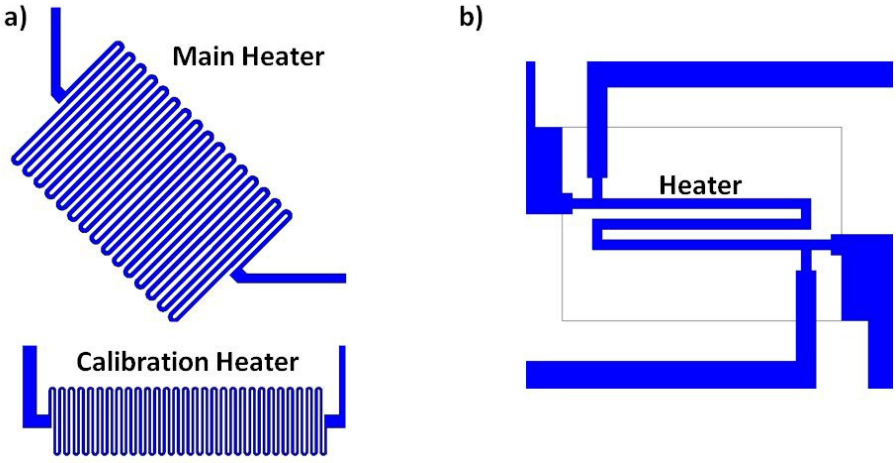

Figure 6 Resistive element shape for prototypes TAMU/ULL-03 and -04.

Figure 7 shows the estimated temperature distributions for TAMU/ULL calorimeter prototypes. As it can be observed, the temperature gradients in the plane *x-y* inside the membrane area are more homogeneous in prototype TAMU/ULL-03. In this figure the height of the plot represents the temperature gradients. Flat profiles are preferred because the heat generated in the resistive layer is evenly transferred to the sample and the RTD sensor (located at the center of the membrane). In the case of prototype TAMU/ULL-04, the heater layout leads to larger temperature gradients.

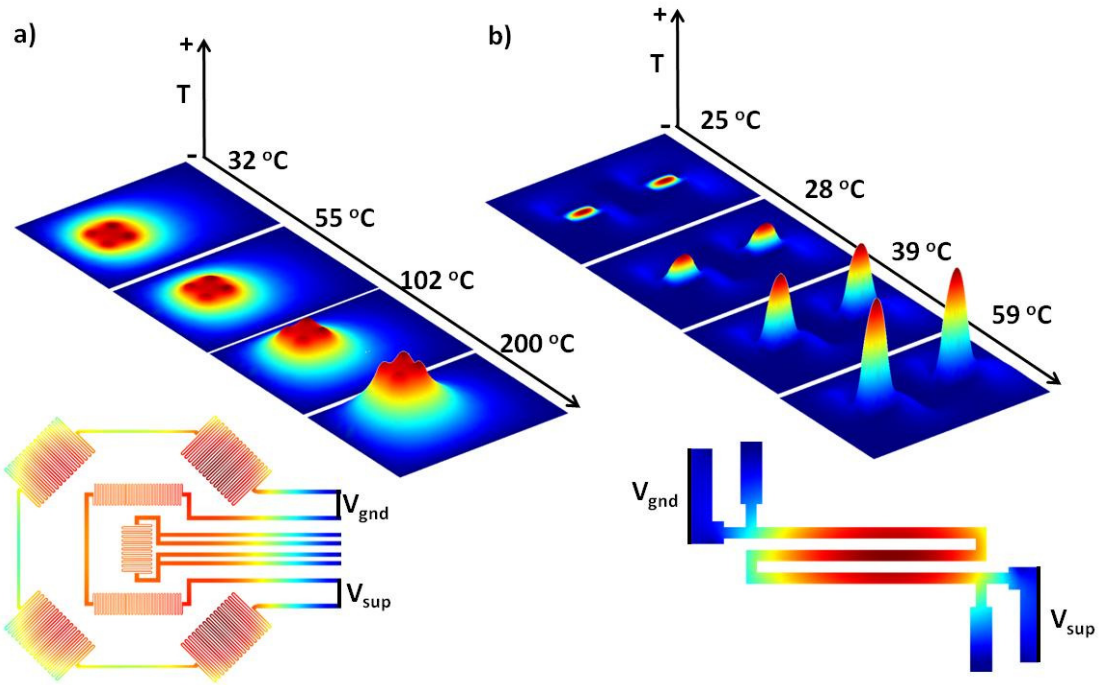

Figure 7 Estimated temperature distributions for prototypes (a) TAMU/ULL-03 and (b) TAMU/ULL-04. Heater details show the distribution of the resultant potential differential when a current is applied to the heaters.

3.3.3 Resistive temperature detectors

Design considerations for the temperature detectors are similar to the ones for the thin-film resistive heaters. The fabrication materials should be capable to work in the temperature range of interest, and their resistivity should have a linear variation as a function of temperature. For the RTDs used in this work, we follow the design proposed by Liu et al.[1, 37], where the temperature detection is performed using 4-wire resistive temperature detectors with meander pattern as the one shown in Figure 8. It has been reported that the

architecture and geometry of thin-film RTDs affects their response [52]. However, further investigation about this subject was beyond the scope of this work and here only one RTD design was studied.

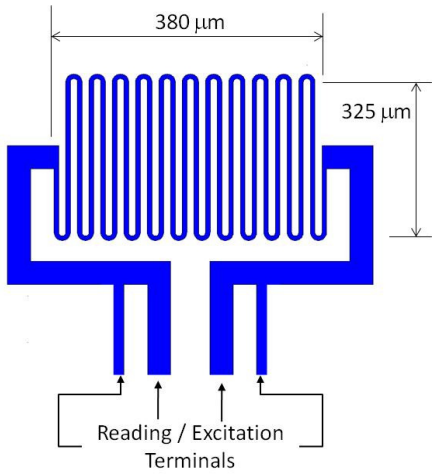

Figure 8 4-wires RTD temperature sensor. The sensors have a resistance of 200 ohm at room temperature and an estimated TCR equal to 0.4%/^{o}C.

One aspect that needs careful considerations in designing the temperature sensor for the calorimeter is its operational principle. RTDs respond to a temperature change with an equivalent change in resistance. However, its operation requires an excitation current and consequently a given amount of power will be dissipated by the thin-film resistance according to equation 4.1, and transferred to the calorimeter surface. For this application, this is particularly important because the amount of heat measured is small. Therefore, the current supplied to the RTDs has to be reduced to prevent self heating, whereas

maintaining an acceptable reading output. Figure 9 shows how the excitation current affects the reading stability of the RTD. For prototype TAMU/ULL-03, an excitation current of 1mA gives a stability of ±0.0375 ohms, which is equivalent to ±0.005^{o}C for temperature readings. With this excitation current self heating was negligible. When the thin-film resistors are used simultaneously as heaters and temperature sensors ($i.e.$, TAMU/ULL-03), the stability of the readings will vary depending on the power supplied.

In the case of the commercial calorimeters developed by Xensor Integration, the temperature sensing is done using thermopiles. This is because thermopiles have the advantage of generating its own electromotive force (emf) and does not need a bias power supply as the RTD. Therefore, no self-heating or other thermoelectric effects occur when operating a thermopile [25], and there is no need to make corrections in the signal due to the heat contribution from the RTD. One disadvantage is that contrary to RTDs that can sense temperatures above 300^{o}C in TAMU/ULL prototypes, the operating range of the thermopiles of Xensor devices is around 100^{o}C due to shifts in the output signal.

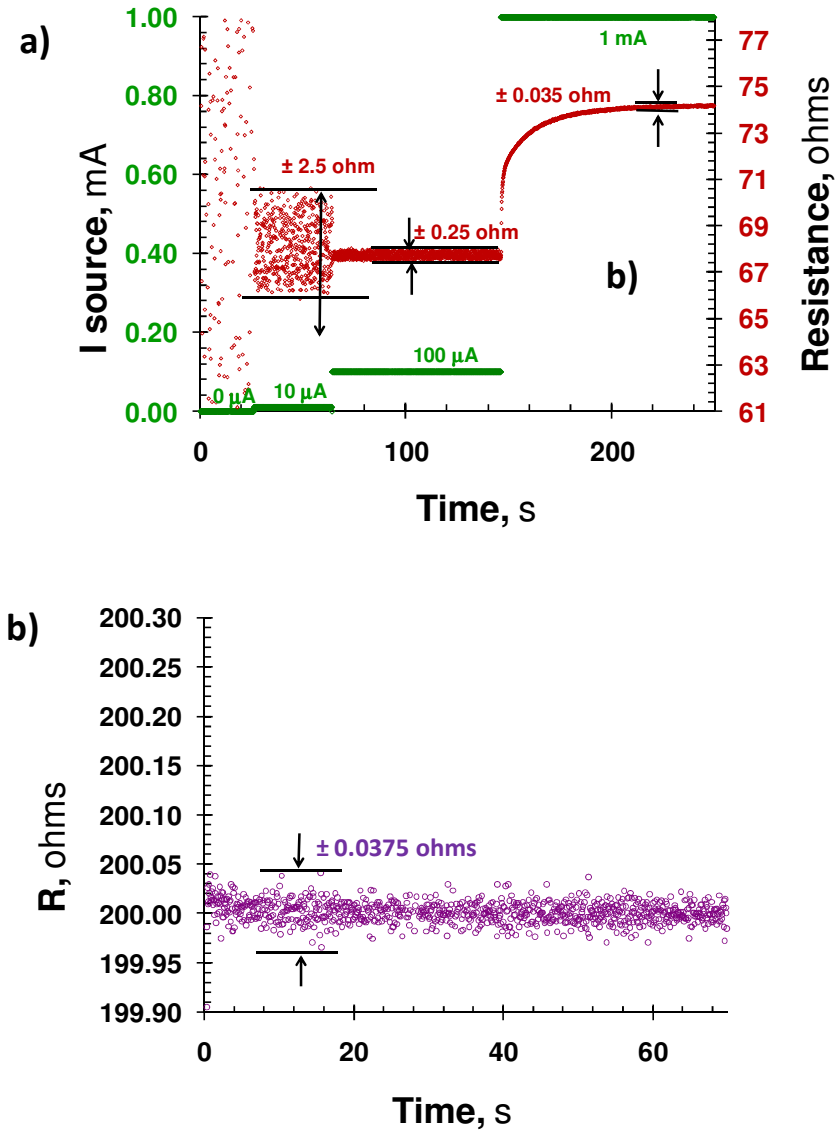

Figure 9 a) Experimental RTD response using different excitation currents for prototype TAMU/ULL-04. b) RTD response of prototype TAMU/ULL-03 using an excitation current of 1 mA.

The sensitivity of the RTDs was characterized through their temperature coefficient of resistance (TCR). Its value represents the sensitivity of the sensor resistance to a change in temperature and can be estimated from the following equation [52]:

$$\boldsymbol{TCR_{RTD}} = \frac{\boldsymbol{R_{100}-R_0}}{\boldsymbol{100\times R_0}} \times \mathbf{100} \tag{3.3}$$

where TCR_{RTD} is the sensor's temperature coefficient of resistance (%/^{o}C); R_{100} is the sensor resistance at 100^{o}C (ohm); and R_0 is the sensor resistance at 0^{o}C (ohm). TCR values were determined both calculated and experimentally.

Calculated TCR values were estimated using the models constructed in COMSOL Multiphysics. In these models the geometry of the RTDs and the excitation current flowing through them were maintained constant. The heat supplied through the electrical heaters was varied to increase the surface temperature of the calorimeter chip. Then, the change in resistance was recorded and the TCR values were estimated using the equation shown above (Figure 10). The averaged TCR calculated in this way was 0.4 %/^{o}C are in very good agreement with the values obtained experimentally during the sensor calibration (see Section 5.3).

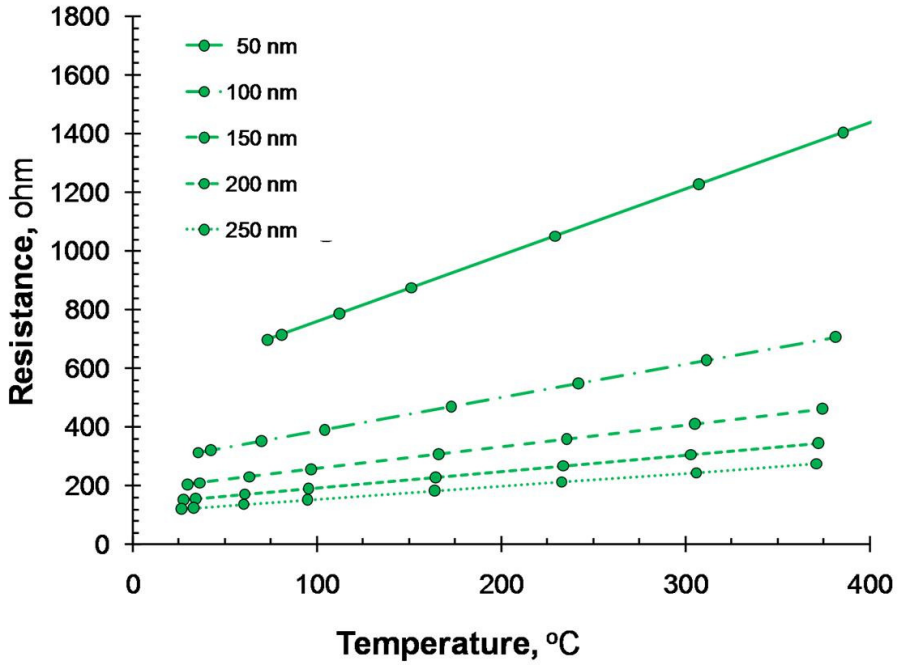

Figure 10 RTD sensor (TAMU/ULL-03) response as a function of temperature and metallization thickness obtained from 2D FEA models.

3.3.4 Bonding pads

The interconnections between the circuit leads in the calorimeter chip and the PCB/chip carrier are typically made using Al wires (D= 20 μm) that are welded to the surface of the bonding pads. The dimensions of the bonding pads/circuit leads have to be considered in the design because they can contribute to the overall calorimeter addenda by adding mass to the device, and provide highly conductive paths for heat losses from the heated area (middle of the membrane) to the silicon frame of the device.

3.4 Thermal resistance

The thermal resistance expressed in units of K/W depicts the spread of heat through the different material layers forming the calorimeter. These layers include bonding pads; membrane; silicon oxide; and adhesive layers. The thermal resistance can be expressed as:

$$\boldsymbol{R_{Th}} = \frac{\boldsymbol{\Delta T}}{\boldsymbol{q_x}} = \frac{\boldsymbol{L}}{\boldsymbol{k \times A_c}} \tag{3.4}$$

The thermal resistance is dependent on the length along the heat flow path or characteristic length (L); the thermal conductivity of the material (k); and the cross sectional area that is available for the heat conduction [51]. From this expression, it is clear that chip-scale calorimeters with thin membranes will have larger thermal resistances. For example, TCG-3880 gauges have a calculated thermal resistance in air of around 30kK/W, whereas TAMU/ULL prototypes and NCM-9924 have thermal resistances in the order of 50-200K/W. This difference in thermal resistance is noticed in the sensitivity of the devices and the power required for the operation of these calorimeters.

4. PROTOTYPES FABRICATION

This section describes the experimental procedures used to fabricate the calorimeter sensor, printed circuit board (PCB); test chambers, and related hardware required to operate the device.

4.1 Micro calorimeter fabrication

The prototype calorimeters used in this work were fabricated in the Materials Characterization Facility (MCF) at Texas A&M University and the Center for Advanced Microstructures and Devices (CAMD) at Louisiana State University. Prime grade double-side polished p-type Si wafers (100) with silicon oxide (200 nm) on the topside and silicon nitride (100 nm) on both sides were used as substrate for the sensor fabrication (Addison Engineering Inc.). The fabrication steps included: backside lithography for membrane pattern transfer (Figure 11b); back-side reactive ion etching (Figure 11c); top-side lithography for heater/thermometers pattern transfer (Figure 11d); vapor deposition of pure aluminum or chromium/gold (Figure 11e); lift-off (Figure 11f); and anisotropic wet etching in an aqueous solution of potassium hydroxide at 85^{o}C (Figure 11g). Prior to the wet etching step, the edge and the upper side of the wafer were protected by a special PEEK wafer holder. A detailed fabrication procedure is given below.

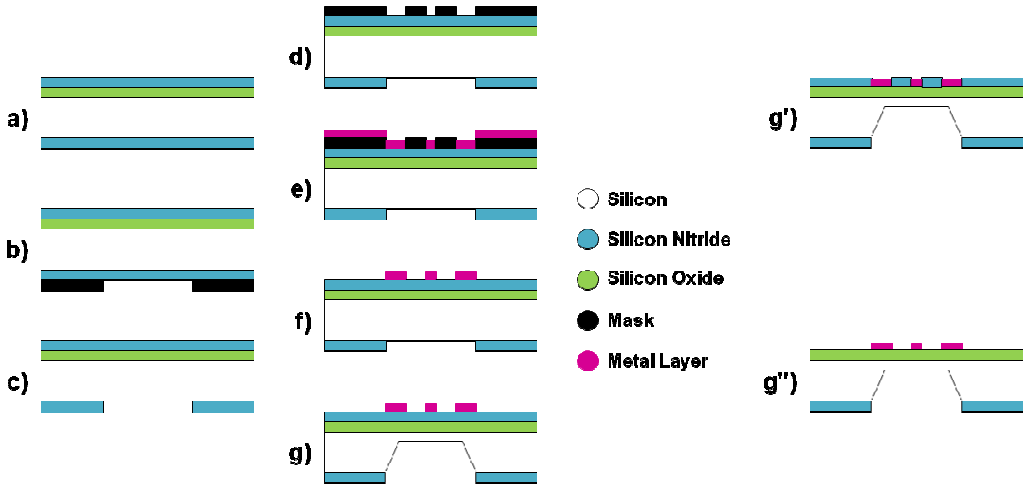

Figure 11 Simplified processing steps for the fabrication of the calorimeters used in this work.

1. *Cleaning:* The wafers were blown with nitrogen to remove any trace of dust, and then rinsed with acetone, isopropyl alcohol, and deionized water. The wafers were immediately dried using nitrogen.
2. *Surface preparation:* The wafers were dried in a hotplate at 90-100^{o}C for 30-60 minutes to remove moisture because it prevents good photoresist adhesion.
3. *Photoresist spin coating*: Both sides of the wafer were spin-coated (Laurell WS-650S) with photoresist shipley-1827 to protect them during the handling of the wafer. After each coating of photoresist, the wafers were soft baked in a hotplate at 90^{o}C for 1.5 minutes.
4. *Pattern transfer (Backside):* The pattern of the membrane was transferred to the backside of the wafer using a Quintel UV exposure station (Quintel

UL7000-OBS mask aligner).The exposure time was set according to the dose recommended for the S1800 series photoresist. The wafer was developed using shipley-351 diluted solution for 30 sec.

5. *Reactive ion etching (RIE):* the exposed part of the silicon nitride on the back side of the wafer was etched away by reactive ion etching (March Plasma Systems CS-1701) using CF_4 as etching gas at a power of 150 Watts for 200 seconds. After this step the wafer was cleaned and dried according to steps 1 and 2.
6. *Pattern transfer (Front Side):* Steps 3 and 4 were repeated and the pattern of the heaters and temperature sensors were transferred to the front side of the wafer using the Quintel UV exposure station.
7. *Metal deposition:* a metal layer is deposited on the front side of the wafer using a metal evaporation chamber (BOC Edwards Auto 306). The material used for the metallization was aluminum or chromium/gold. The thickness of the layer was defined by the desired heater/RTD resistance. After deposition the photoresist and the excess of metal were removed by lift-off using acetone as a solvent.
8. *Front side protection*: The electronics' side of the wafer was protected by a special PEEK wafer holder that prevented any liquid to get in contact with it.
9. The back side of the wafer was etched in a 35 wt% KOH aqueous solution at 80℃ to remove the silicon exposed during the RIE step. This step is used to create the membranes in the sensor structure. The exposure time and

conditions for the anisotropic etching process were carefully controlled to produce membranes of several microns thick (10, 50 and 100 μm).

10. Individual calorimeter sensors were diced using an automatic diamond blade and then connected to a PCB either by wire bonding (Kulicke & Soffa Ltd.) or by mechanical contact using standard pogo pins, depending on the sensor design.

The fabrication procedures can be adapted to produce sensors, which electronics side is directly on the silicon oxide layer (Figure 11g'), or embedded in the etched cavities of the silicon nitride layer (Figure 11g'').

4.2 Printed circuit board

The PCB used to connect the calorimeters to the hardware and DAQ were fabricated using positive photoresist pre-sensitized phenolic PCBs (Kinsten). The fabrication started by transferring the desired circuit pattern to the pre-sensitized PCBs by exposing it to UV light through a mask. Then, the PCB was developed in a NaOH dilute solution (3.5 ml of NaOH@50% and 500 ml H_2O). Finally, the exposed area of the PCB was etched using ammonium persulphate solution (75 g and 500 ml H_2O) at 40-50 ºC. Finally, the photoresist was removed using acetone at room temperature.

5. EXPERIMENTAL

5.1 Experimental setup

The experimental setup for testing the chip-scale calorimeters used in this work consisted of the following components:

Testing chamber – This chamber allows conducting experiments under a controlled atmosphere using air, nitrogen or vacuum. When the experiments were performed under air atmosphere, the chamber acted simply to reduce signal fluctuations due to thermal disturbances from the surroundings. Figure 12 shows the chamber used for testing a single calorimeter, but using two calorimeters simultaneously is also possible.

Aluminum block – The function of the aluminum block is to act as a thermostat to dissipate the heat that is transmitted through the chip-carrier or PCB. This is important to maintain the temperature of the areas outside the membrane close to room temperature.

Power source – The electrical power for the resistive heaters in the calorimeters is supplied either by two 16-bit programmable DC power supplies (NI PXI-4100), or a high-resolution custom-made constant power supply, depending on the experiment requirements.

Data collection – A sensing system consisting of $6^1/_2$ digital multimeters with a flexible resolution of 10 to 23-bits (NI PXI-4070) was used to measure the

thermopiles and RTDs outputs. In addition, a 16-bit 4-wire RTD module (NI FP-RTD-124) was also used for measuring the output from the RTDs.

Software interface – The data acquisition and the control algorithm for the chip-scale calorimeters were implemented using LabView™. The customized LabView™ program and hardware allows multiple operation modes including temperature ramps with a feedback control with variable gains, programmable time-dependent voltage mode, programmable time-dependent current mode, and isothermal mode.

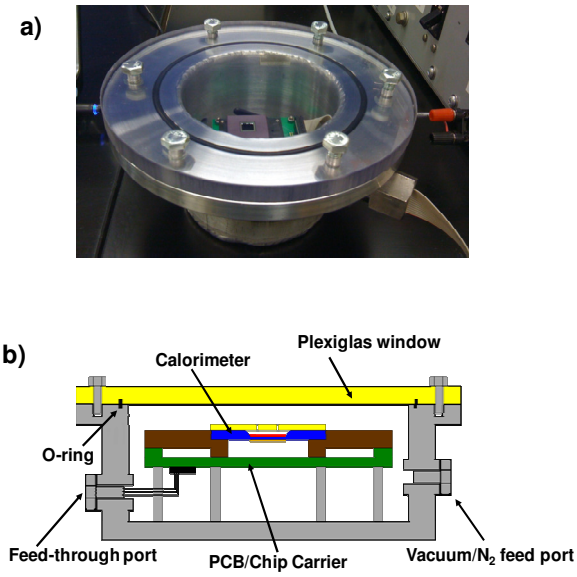

Figure 12 a) Test chamber for performing the experiments using different types of calorimeters. b) Schematic drawing showing the chamber components.

5.2 Temperature control

The temperature program used in the experiments was linear with time, or under isothermal mode when indicated. A PID temperature control was implemented in LabView™ to regulate the power supplied to the heaters. The control received temperature feedback from the RTD sensors, which are previously calibrated as described in Section 5.3. In the case of Xensor devices, the temperature information can be obtained from their thermopiles. Using thermopiles as temperature sensor have the advantage that they do not need a bias power supply as the RTDs. Therefore, no self-heating or other thermoelectric effects occur when operating a thermopile [25]. In addition, thermopiles provide fast time responses. However, as mentioned before, the maximum operating range of thermopiles in sensors LCM-9924 and LCM-2506 was limited to around 100^{o}C.

5.3 Temperature sensor calibration

Before performing experiments, the RTDs were calibrated against an external and commercially available thin-film RTD (F3105 from Omega), by placing the calorimeter and the reference RTD in an oven and recording the resistance of the RTDs as a function of the temperature (R(T)). The calibration temperature was fixed depending on the expected maximum temperature for each experiment. Table 3 shows the resistance values used for the TCR estimation for prototype TAMU/ULL-03 collected using three different devices.

Resistance values at 100°C were obtained directly during the calibration process, whereas resistance values at 0°C were obtained by extrapolation of the R(T) data set. The TCR values were calculated according to equation given in page 28.

Table 3 RTD temperature coefficients of resistance obtained experimentally for three different devices with the same design (TAMU/ULL-03) fabricated in the same wafer.

Device	**R(0°C), ohm**	**R(100°C), ohm**	**TCR_{exp}, %/°C**
I	199.1	204.5	0.42
II	198.9	207.2	0.41
III	198.9	206.9	0.40
		Average TCR	0.41

Figure 13 shows a snapshot of the LabView™ routine created to carry out the calibration of the sensors. The routine automatically collects the temperature readings from the external calibration RTD and the resistance values of the calorimeter RTD. This subroutine also allows selecting which data is used for the estimation of R(T), visualizing the corresponding equation (linear or quadratic), and saving the calibration data into an ASCII file.

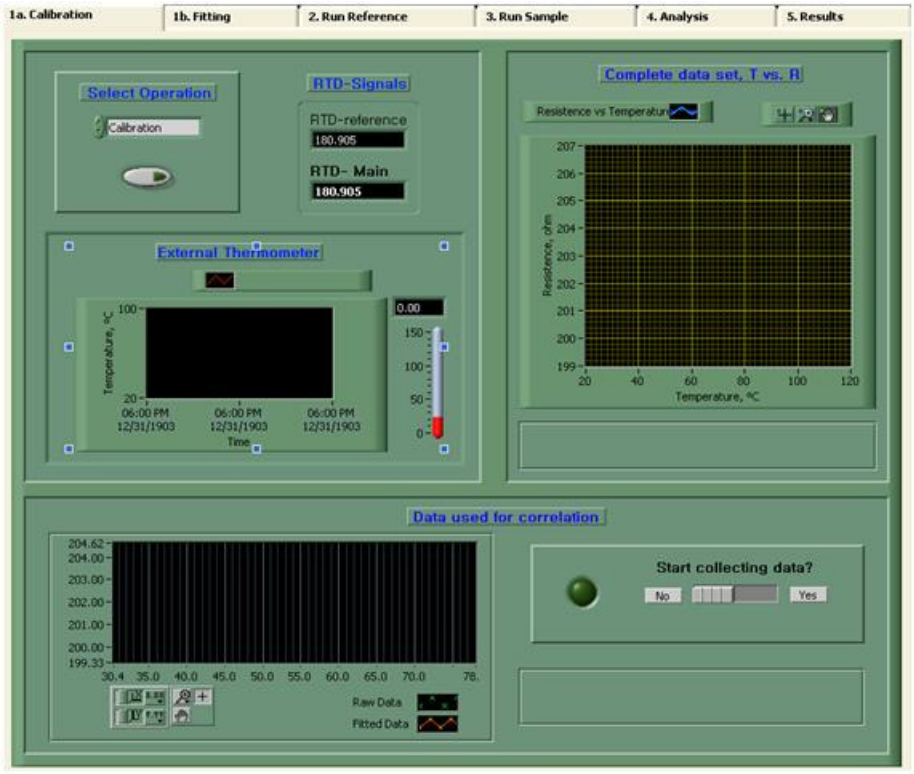

Figure 13 Screen shot of the LabView™ subroutine used for the RTD calibration.

The calibration of the sensors was verified by determining the transition temperature of indium. This material was selected because it is a very known calorimetric standard that has a well defined endothermic peak corresponding to its melting transition. For the experiments, a minute amount of indium (Sigma-Aldrich) in the form of fine powder was placed in the cavity created beneath the calorimeter membrane. The sample was heated until melted several times to form a thin layer on the surface of the heated area in the membrane. This was

done to have a well defined endothermic peak. Notice that for the design of chip-scale calorimeters, the uniformity of the heated area is critical for obtaining acceptable results. The peak definition depends on an adequate sample/sensor contact. Transition lags may appear if the sample is not heated evenly due to temperature gradients. Figure 14 shows the raw data obtained experimentally and the time-averaged values. The transition temperature measured with the RTD was then adjusted with the expected temperature from literature.

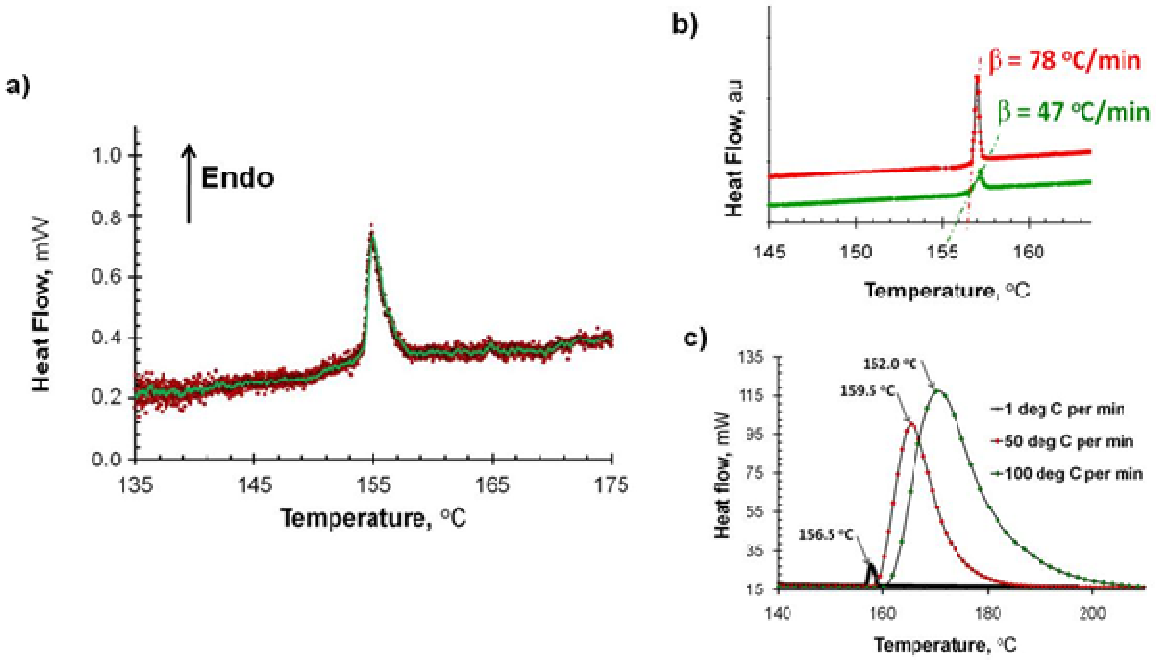

Figure 14 Thermogram of the thermal transition of pure indium obtained with TAMU/ULL-03 prototype showing the differential (dots) and the time averaged signal (continuous line) [53].

5.4 Application examples using liquid samples

Chip-scale calorimeters with membranes of 10-50 μm are relatively strong for use with liquid samples. The membrane acts a physical barrier that separates the electronic side of the calorimeter from the sample and the hollow space acts as sample reservoir with a known volume. By using this cavity, the use of micro channels is not required and the sample can be simply injected through micro holes drilled on a glass cover (see Figure 15a). For this work the glass covers were drilled using spark assisted chemical engraving (SACE). This procedure was done in an aqueous solution of NaOH (30 wt. %) at room temperature using an electrode connected to a VDC source. Details about spark assisted chemical engraving are not discussed here, but can be found elsewhere [54-55].

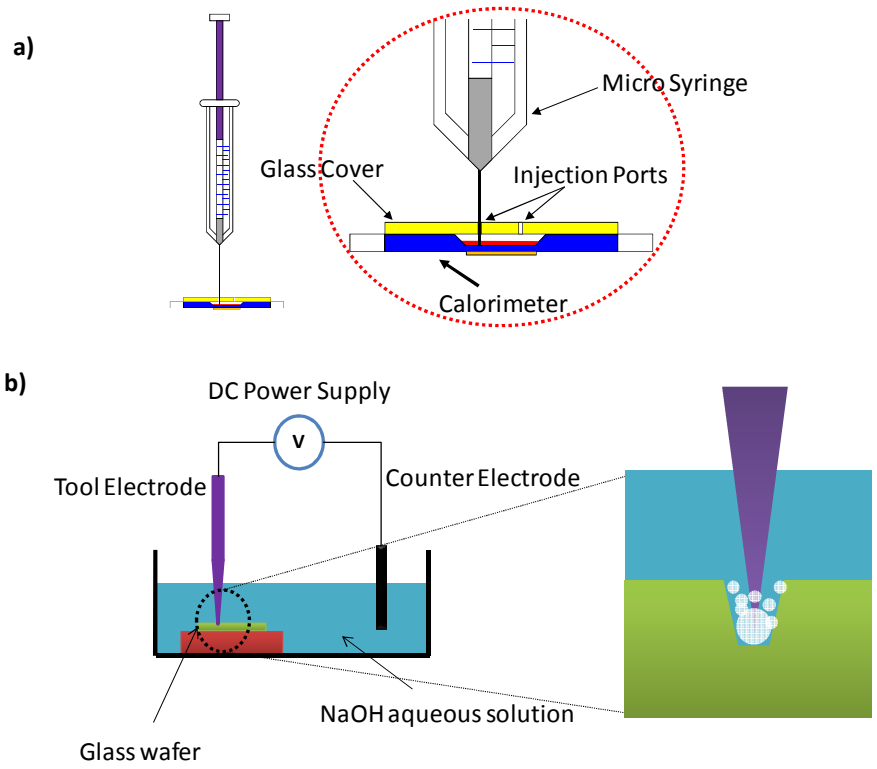

Figure 15 a) Schematic representation of the experimental setup used for using the chip-scale calorimeters with liquid samples. b) SACE procedure used for the fabrication of the injection port in the glass covers.

5.4.1 Evaporation of acetone

The evaporation of acetone was determined using a TAMU/ULL-03a prototype. The experiment started with the sample injection using a micro syringe and keeping the sample at the desired temperature (total volume included glass cover ~25 μL). Then, the perforated holes allowed free

evaporation of the sample. The area of the heat required by the controller was related to the enthalpy of vaporization. The averaged heat of vaporization determined at 30°C was 384 J/g, which differs from the literature value of 550 J/g. This difference is attributed to uncertainties during the sample injection and the calibration process [53]. Figure 16 shows a thermogram obtained following the procedure described above. Further work needs to be done to improve the control and methods to reduce this error.

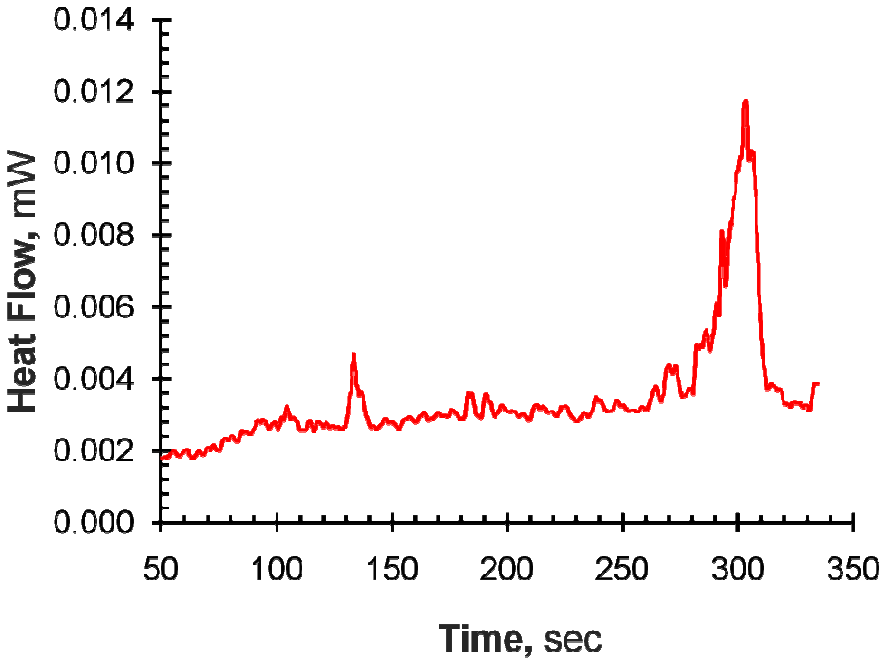

Figure 16 a) Thermogram of the evaporation of acetone obtained with calorimeter TAMU/ULL-03a [53].

5.4.2 Heat of mixing (HOM) screening

Chip-scale calorimeters based on thick-membranes are ideal for screening liquid samples for changes in energy due to the mixture between two samples. From an application point of view, chip calorimeters can be used to fabricate handheld devices which can be deployed on field applications for safety screening of liquid mixtures. In order to illustrate this application, LCM-2506 and NCM-9924 liquid nanocalorimeters were used to screen two binary mixtures to determine the release or absorption of energy when the individual components are combined.

These calorimeters can be also operated in isothermal mode to monitor HOM. Using the same experimental setup shown in Figure 15a, a microsyringe can be used to inject two liquid samples. Then, the heat evolved or absorbed during the process can be related to the change in the output from the calorimeter sensor. Figure 17 shows a qualitative determination of the HOM for the mixture of benzene/ethanol. This mixture was selected because there are results reported in the literature using traditional scanning calorimeters that can be used as reference. The experiment started by adding benzene into the calorimeter, and maintaining an electrical power to produce a temperature of around 30^{o}C, and the changes in the resistance of the sensor was monitored. Then successive injections of ethanol were performed and the sensor output was recorded. The results obtained using LCM-2506 liquid nanocalorimeter (Figure 17a) showed similar trend reported by Mita et al [56]. The sensor output

was smaller for successive higher concentrations of ethanol. Figure 17b shows the results obtained with a NCM-9924 liquid nanocalorimeter when different amounts of ethanol are added to 20 μL of benzene. These results show an endothermic behavior when benzene and ethanol are mixed together.

In a different experiment, a mixture of pyridine and acetic acid was prepared as an example of an exothermic HOM. In this case, pyridine was injected to a NCM-9924 containing acetic acid at around 40^{o}C. As can be observed in Figure 18, the first peak occurs when the acetic acid is injected, then subsequent peaks are related to the addition of pyridine. The magnitude of the HOM decreases as the concentration of pyridine in acetic acid increases, and contrary to the benzene/ethanol case, here the results revealed an exothermic behavior.

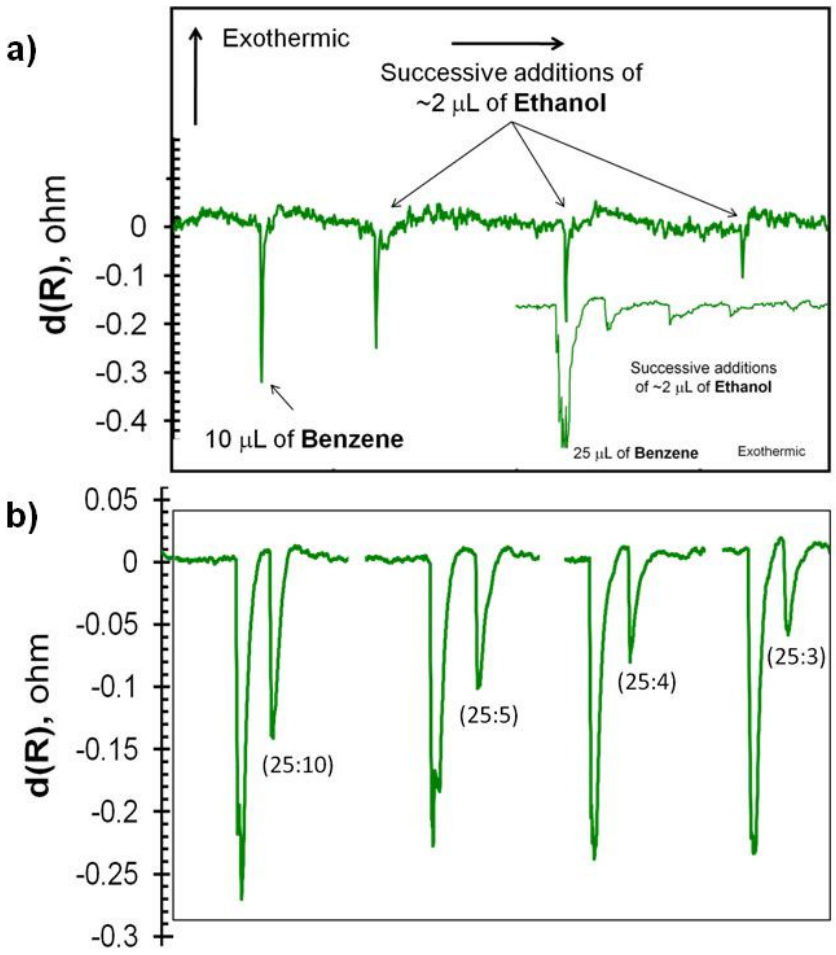

Figure 17 Thermograms obtained for screening the heat released when benzene and ethanol are mixed together. a) Results obtained using a LCM-2506 liquid calorimeter. The insert was obtained with a NCM-9924 calorimeter. b) Addition of ethanol (10, 5, 4, and 3 μL) to 25 μL of benzene in a NCM-9924 calorimeter [53].

These two examples demonstrate that thick-membrane calorimeters are useful to detect changes in energy when two liquid samples are mixed. From an application point of view, handheld devices based on chip calorimeters can be used for safety screening of liquid mixtures in field applications because they will provide a quick result about the behavior of a liquid mixture.

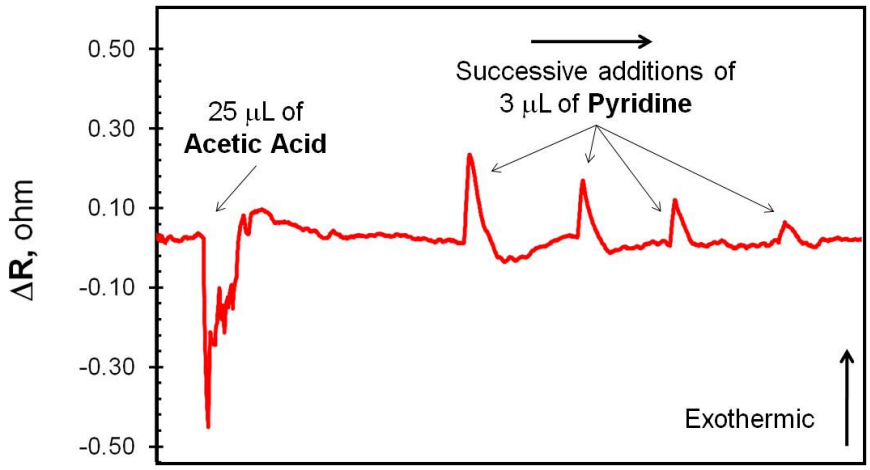

Figure 18 Thermogram obtained with NCM-9924 sensor. Here, 3 μL of pyridine were added successively to an initial volume of 25 μL of acetic acid at 40°C [53].

5.5 Application examples using solid samples

Testing of solid samples with membrane calorimeters is also possible. However, the complexity increases because the tiny amount of sample required is difficult to measure accurately, and because the heat transfer between the heated area of the calorimeter and the sample is more complicated because it is highly dependent on the contact area of the sample and the sensing area. A

common practice for testing solids in nanocalorimeter systems is to place the sample directly over the sensing area of the calorimeter in the form of a thin layer, which is applied using deposition techniques. In this approach, the amount of material is accurately known because the dimensions of the material layer are defined. Using this technique, the heat transfer problem is solved because the thermal contact between the sensing area in the calorimeter and the sample is good. However, this technique is not applicable to all materials, and it is not adequate for devices that have an intended use outside the controlled laboratory environment. For the experiments conducted in this work, the samples were added in powdered form and the amount of sample was approximated from the volume of the cavity beneath the calorimeter membranes. Therefore, the release/absorption of energy was done in relative terms.

Regarding the heat transfer, good thermal contact between the sample and the sensing area is important to transfer the heat generated in the heaters to the sample. Thermal conductivity, area of contact, and thickness of the sample, control the effectiveness of the heat transfer and the size of the sample and heating rates that can be used for the analysis using chip-scale calorimeters. Figure 19 shows calculated temperature distributions of a hypothetical sample with spherical shape. The shape of this hypothetical sample was selected because it represents the worst case where there are very little contact area between the sample and the heated area in the calorimeter. From these model results, it is clear that when the material has low thermal conductivity the layer of

sample needs to be very thin (<200 μm) to avoid large temperature gradients and be able to operate at high heating rates above. The following section describes two application examples using solid samples.

5.5.1 Thermal screening of gunpowder

A typical application of calorimetry is the thermal hazard assessment of chemical reactions. The determination of heat of reactions is commonly carried out in differential scanning calorimeters. However, in the presence of highly energetic materials, experiments using traditional calorimeters are not trivial due to the potential high energy release from the decomposition reaction that can damage the equipment during testing. The reduced sample required by chip-scale calorimeters will allow performing thermal analyses of highly energetic materials in a safe way. It is expected that the unique characteristics of chip-scale calorimeters can be used to produce handheld calorimeters for the screening and detection of highly energetic substances in security applications [1, 37]. As explained before such handheld calorimeters will be very useful to detect hazardous energetic materials. A simple test in a scanning calorimeter can reveal if an unknown sample is a thermal hazard.

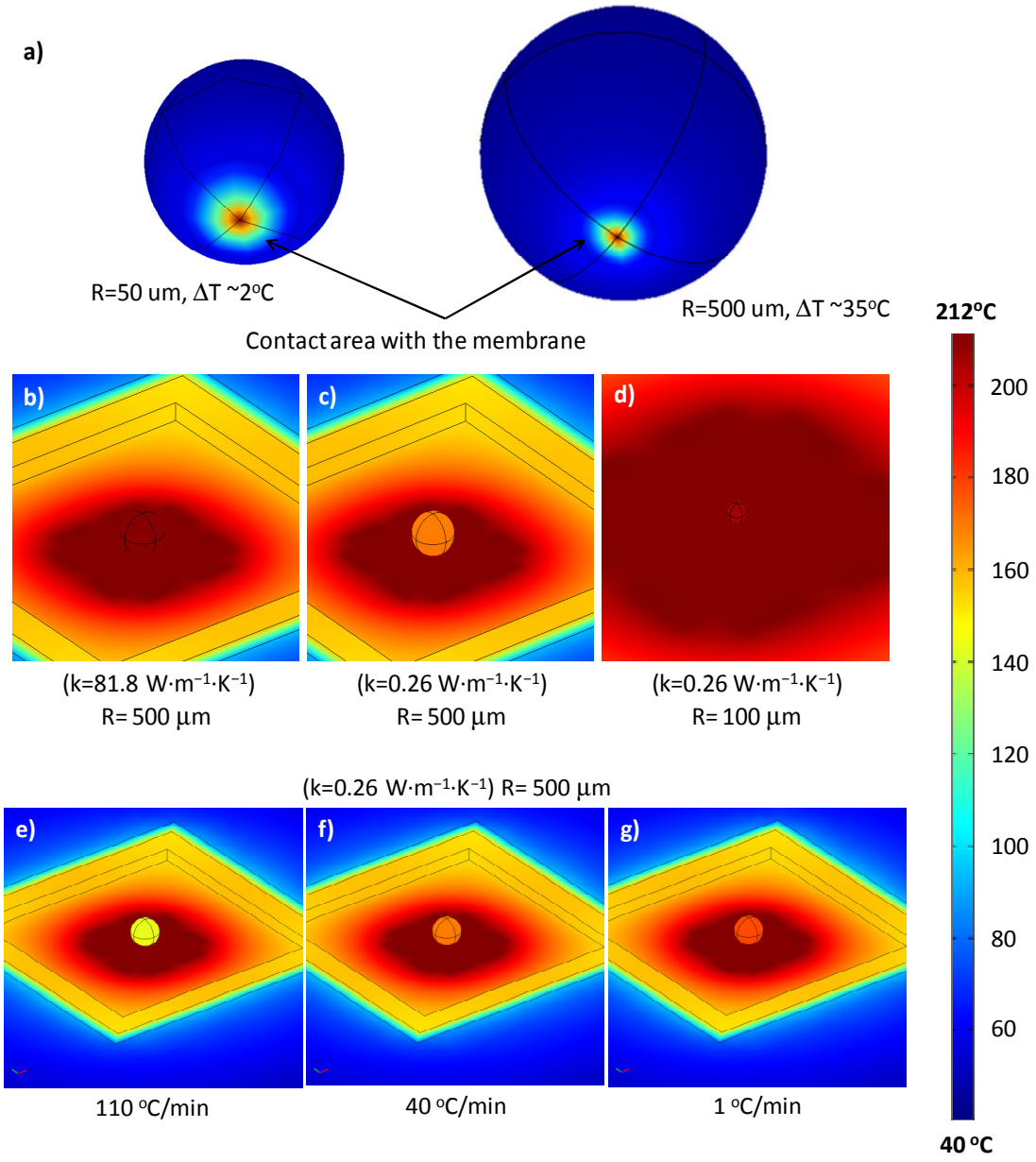

Figure 19 a) Temperature difference between the coldest side of a spherical sample and the membrane; b) effect of thermal conductivity and sample size; and c) effect of heating rate on the sample temperature.

In this work we used one of our prototypes (TAMU/ULL-04b) to perform a thermal screening of a gunpowder sample (Remington). This material was selected because it is easily available, and moreover because it can give an idea about the performance of the prototypes when used with energetic materials. Also, the individual grains of the gunpowder sample are almost spherical (D~200 μm). In this way, it was possible to observe the case where the contact between the sample and the heated area in the calorimeter is not good. For this sample, the experimental setup was slightly modified in order to prevent the rupture of the calorimeter membrane due to the gases generated during the decomposition of the sample. The glass cover placed over the membrane-side of the calorimeter was not glued to allow the gasses to escape. Therefore, the experiments were conducted in a cell not closed hermetically Figure 20 shows the differential signal obtained experimentally using a gunpowder sample. Here, the power supplied to the heaters was increased linearly to produce a heating rate of around 25^{o}C/min. The result obtained revealed a sharp exotherm that was in excellent agreement with the thermogram obtained with a traditional DSC. The response of the sensor to a rapid event was successful and the prototype was able to capture the sharp exothermic decomposition of gunpowder.

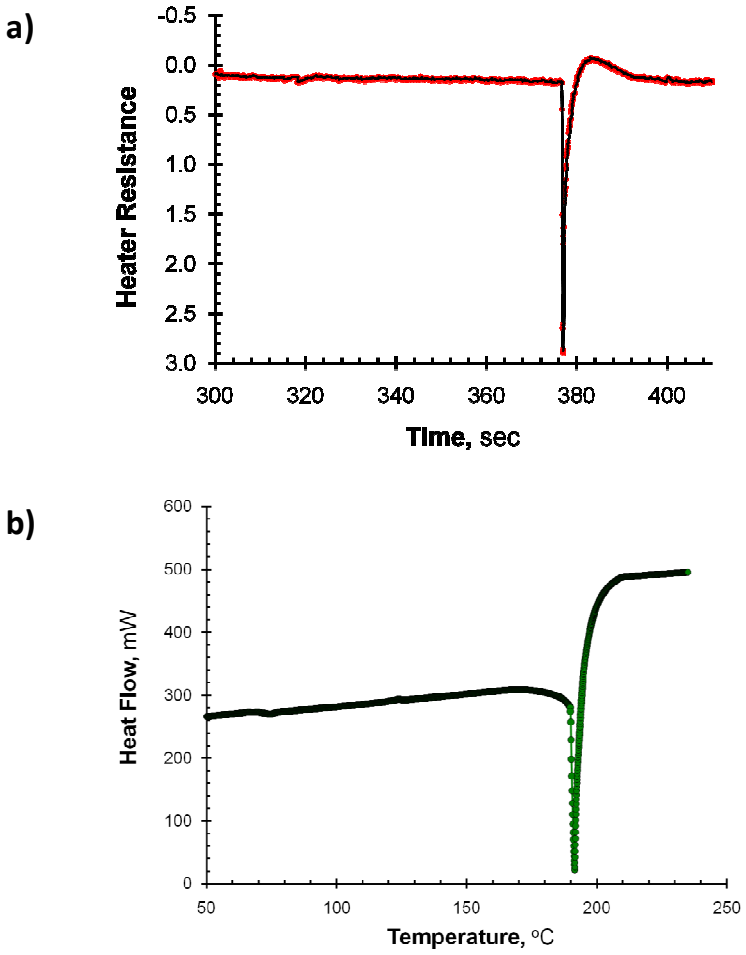

Figure 20 a) Differential signal output obtained using a prototype calorimeter TAMU/ULL-04b with gunpowder sample. The insert show the results obtained using a conventional DSC (Pyris, from Perking Elmer) [53].

5.5.2 Thermal screening of picric acid

As mentioned at the beginning of this section, the heating rates that can be used with chip-scale calorimeters are very dependent on the thermal mass of the device, and the effectiveness of the heat transfer between the calorimeter and the sample. Calorimeters with thick membranes (10-50 μm) can be used at maximum heating rates around 100-200°C/min. On the other hand, if faster heating rates are required, thin-film calorimeters are a desirable alternative. As an example, TCG-3880 gauges (Xensor Integration) are devices with very low thermal mass. Therefore, they can be used to perform analysis at very high heating rates using very tiny samples with minimum power consumption. Figure 21 shows the calculated and experimental values of the sensor temperature as a function of the applied voltage. As an example of the use of this senosors, Figure 22 shows a thermogram obtained from a picric acid sample. For the analysis, a needle-sized sample was placed over the heated area of the TCG-3880 gauge using an optical microscope. The gauge temperature was then raised by quickly increasing the voltage across the resistive heater following a linear ramp. The experiment was conducted according to the procedure used by Zuck et al [40]. For comparative purposes a thermogram obtained with a conventional DSC using a closed cell is shown in the figure insert. As it can be observed, the result obtained with the TCG-3880 agrees with the thermogram obtaining using a commercial DSC, and the endothermic/exothermic transitions were successfully identified.

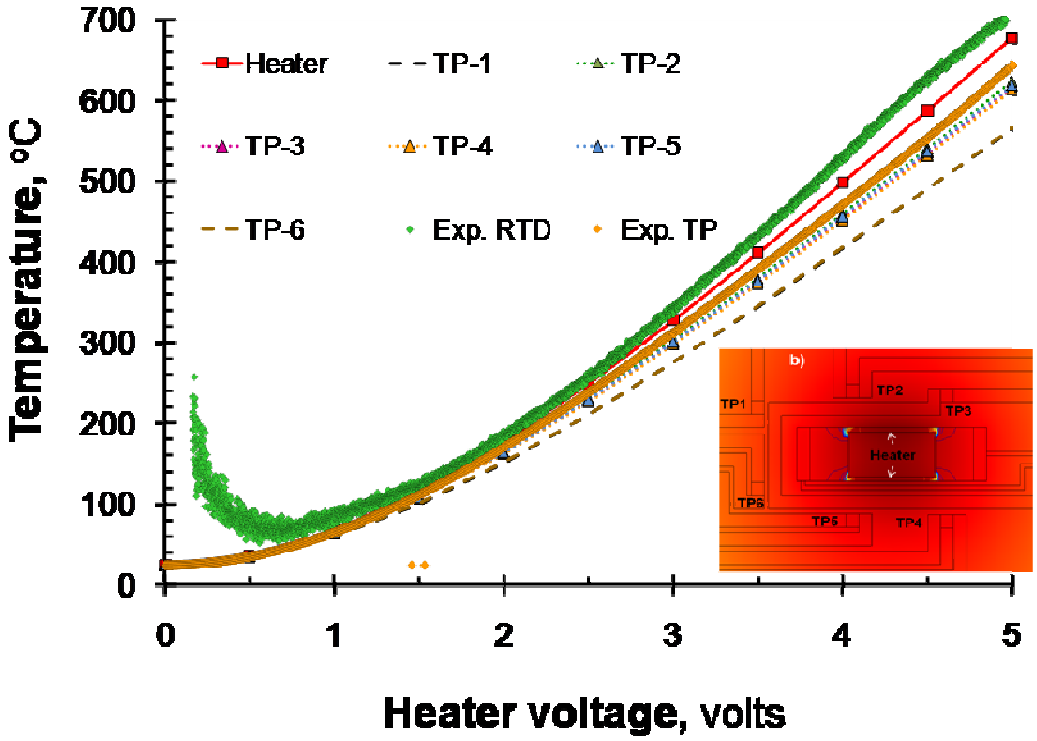

Figure 21 TCG-3880 gauge's temperature as a function of the applied voltage and position. Green dots are experimental values measured with the change in resistance of the poly-Si heater. The orange dots are the temperature measured using the gauge's thermopile. The rest of the values were obtained using FEA.

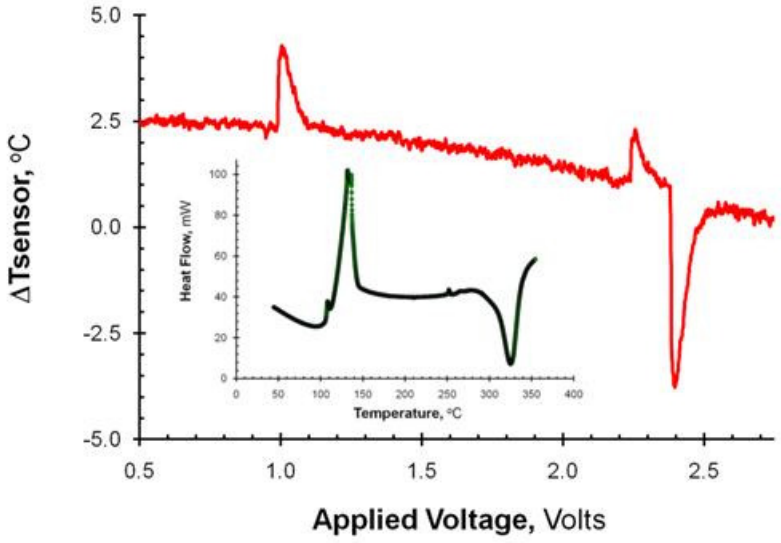

Figure 22 Differential signal obtained using a TCG-3880 sensor for the screening of impure picric acid. The insert shows the result obtained using a conventional DSC [53].

6. CONCLUSIONS AND FUTURE RESEARCH PATHS

6.1 Conclusions

Thermal analysis of unknown samples provides information about the energy released during their thermal decomposition. Therefore, calorimetric methods can be used as a novel approach for detection of highly energetic materials with the potential of being an explosive hazard. However, to date, no commercial calorimeter can satisfy the features required to be used as an explosive detector. In this work we have designed and fabricated two chip-scale calorimeters based on thick silicon membranes that can be used for thermal screening of microscale samples. The use of thick membranes has a negative impact on the sensitivity of the device. However, the mechanical strength is improved, which makes more robust devices that are strong enough to be deployed outside the laboratory environment. This feature opens the possibility to be incorporated into portable (handheld) systems that can be deployed in field applications. Despite their lower sensitivity in relation to thin-film film nanocalorimeters, we have shown that the calorimeters presented here, based on thick membranes, can successfully detect the thermal transition of a number of different liquid and solid samples. Also their potential to be used with energetic materials was demonstrated by detecting the rapid decomposition of a gunpowder sample in a semi-confined environment. With this work, it is expected that that the knowledge gained in this work can rapidly be applied to

the development of a final device that can be tested under real test conditions for a variety of controlled substances.

6.2 Future work

The work presented here focused on the design of chip-scale calorimeters prototypes based on thick-membrane silicon technology. These sensors were successfully tested with gunpowder and the results obtained agreed with previous literature. However, the use of these sensors under real conditions requires additional work, which needs to be completed before chip-scale calorimeters can be used in commercial applications. The following research tasks are expected to produce a tool with the required characteristics of a handheld device for the thermal screening and detection of energetic materials.

Sensor geometry optimization: The sensing part of the calorimeter is located in its membrane, which is supported on a silicon rim that serves as a heat sink and it is where the bonding pads are located. During this work, the silicon rim was over dimensioned to accommodate large area bonding pads in order to facilitate the wire-bonding operations. The large silicon rim has a positive effect by providing a large area for the contact between the sensor and the heat sink. However, the number of sensors that can be fabricated in a single wafer is reduced and the fabrication costs increases. In large scale production, the wire-bonding operations are fully automated. Therefore, it is possible to reduce the

silicon rim and lower the fabrication costs. A final prototype should take this into account, especially when considering the effect of reducing the contact area with the heat sink on the overall temperature distribution of the sensor and chip carrier.

Automated sampling system: Chip-scale calorimeters with thick membranes are suitable for handling both liquid and solid samples. In the case of liquid samples, the sampling system is relatively straightforward because the sample is injected using a micro syringe or a syringe pump and the sample mass can be determined from the injected volume. However, for solid samples an automated sampling system suitable for handheld devices is not available. This sampling system should take into account an accurate determination of the sample mass, sample thickness, and an enhanced thermal contact between the sample and the membrane of the sensor.

Integrated electronics: The majority of the electronics required to operate and to collect data from the calorimeter used in this work are commercially available, and hence not specifically tailored for this application. Therefore, collaboration with another engineering field such as electrical engineering will be beneficial for the construction of a final calorimetric device. The experience gained with this research and the collected data will help to design and manufacture tailored electronics that can fit into handheld devices.

REFERENCES

[1] Y.-S. Liu, V.M. Ugaz, S.W. North, W.J. Rogers, M.S. Mannan, Development of a miniature calorimeter for identification and detection of explosives and other energetic compounds, Journal of Hazardous Materials, 142 (2007) 662-668.

[2] E.M. Barrall, Precise determination of melting and boiling points by differential thermal analysis and differential scanning calorimetry, Thermochimica Acta, 5 (1973) 377-389.

[3] M.-H. Yuan, C.-M. Shu, A.A. Kossoy, Kinetics and hazards of thermal decomposition of methyl ethyl ketone peroxide by DSC, Thermochimica Acta, 430 (2005) 67-71.

[4] R.J. Seyler, Application fo pressure DTA (DSC) to thermal hazard evaluation, Thermochimica Acta, 39 (1980) 171-180.

[5] C.-P. Lin, C.-P. Chang, Y.-C. Chou, Y.-C. Chu, C.-M. Shu, Modeling solid thermal explosion containment on reactor HNIW and HMX, Journal of Hazardous Materials, 176 (2010) 549-558.

[6] A. Iliyas, K. Hawboldt, F. Khan, Thermal stability investigation of sulfide minerals in DSC, Journal of Hazardous Materials, 178 (2010) 814-822.

[7] D.R. Queen, F. Hellman, Thin film nanocalorimeter for heat capacity measurements of 30 nm films, Review of Scientific Instruments, 80 (2009) 063901-063907.

[8] A.W. van Herwaarden, Overview of calorimeter chips for various applications, Thermochimica Acta, 432 (2005) 192-201.

[9] B. Revaz, B.L. Zink, D. O'Neil, L. Hull, F. Hellman, Numerical simulation of the heat transfer in amorphous silicon nitride membrane-based microcalorimeters, Review of Scientific Instruments, 74 (2003) 4389.

[10] S. Adamovsky, C. Schick, Ultra-fast isothermal calorimetry using thin film sensors, Thermochimica Acta, 415 (2004) 1-7.

[11] S.A. Adamovsky, A.A. Minakov, C. Schick, Scanning microcalorimetry at high cooling rate, Thermochimica Acta, 403 (2003) 55-63.

[12] L.H. Allen, Nanocalorimetry measurements of materials having small dimensions, in: Proceedings of the 5th International Conference on Solid-State and Integrated Circuit Technology, Beijing , China, 21-23 October, 1998, pp. 563.

[13] J. Lerchner, Report on the workshop "Nanocalorimetry", Thermochimica Acta, 337 (1999) 231-233.

[14] J. Lerchner, G. Wolf, C. Auguet, V. Torra, Accuracy in integrated circuit (IC) calorimeters, Thermochimica Acta, 382 (2002) 65-76.

[15] B. Revaz, B.L. Zink, F. Hellman, Si-N membrane-based microcalorimetry: Heat capacity and thermal conductivity of thin films, Thermochimica Acta, 432 (2005) 158-168.

[16] P.M. Sarro, A.W. van Herwaarden, W. van der Vlist, A silicon-silicon nitride membrane fabrication process for smart thermal sensors, Sensors and Actuators A: Physical, 42 (1994) 666-671.

[17] W. Winter, G.W.H. Höhne, Chip-calorimeter for small samples, Thermochimica Acta, 403 (2003) 43-53.

[18] S. Youssef, J. Podlecki, R. Al Asmar, B. Sorli, O. Cyril, A. Foucaran, MEMS Scanning Calorimeter With Serpentine-Shaped Platinum Resistors for Characterizations of Microsamples, Journal of Microelectromechanical Systems, 18 (2009) 414-423.

[19] Z.S. Zhang, O.M. Wilson, M.Y. Efremov, E.A. Olson, P.V. Braun, W. Senaratne, C.K. Ober, M. Zhang, L.H. Allen, Heat capacity measurements of two-dimensional self-assembled hexadecanethiol monolayers on polycrystalline gold, Applied Physics Letters, 84 (2004) 5198-5200.

[20] F. Fominaya, T. Fournier, P. Gandit, J. Chaussy, Nanocalorimeter for high resolution measurements of low temperature heat capacities of thin films, Review of Scientific Instruments, 68 (1997) 419-4195.

[21] M. Zhang, M.Y. Efremov, F. Schiettekatte, E.A. Olson, A.T. Kwan, S.L. Lai, T. Wisleder, J.E. Greene, L.H. Allen, Size-dependent melting point depression of nanostructures: Nanocalorimetric measurements, Physical Review B, 62 (2000) 10548-10557.

[22] A.F. Lopeandia, L.I. Cerdo, M.T. Clavaguera-Mora, L.R. Arana, K.F. Jensen, F.J. Munoz, J. Rodriguez-Viejo, Sensitive power compensated scanning calorimeter for analysis of phase transformations in small samples, Review of Scientific Instruments, 76 (2005) 065104-065105.

[23] V. Baier, R. Födisch, A. Ihring, E. Kessler, J. Lerchner, G. Wolf, J.M. Köhler, M. Nietzsch, M. Krügel, Highly sensitive thermopile heat power sensor for micro-fluid calorimetry of biochemical processes, Sensors and Actuators A: Physical, 123-124 (2005) 354-359.

[24] A.W. Van Herwaarden, P.M. Sarro, J.W. Gardner, P. Bataillard, Liquid and gas micro-calorimeters for (bio)chemical measurements, Sensors and Actuators A: Physical, 43 (1994) 24-30.

[25] E.A. Johannessen, J.M.R. Weaver, P.H. Cobbold, J.M. Cooper, A suspended membrane nanocalorimeter for ultralow volume bioanalysis, IEEE Transactions on NanoBioscience, 1 (2002) 29-36.

[26] T. Weiss, G. Igel, G. Urban, Chip-Based Scanning Nano-Calorimeter for Protein Stability Analysis in Biosensor Membranes, in: Proceedings of the Conference of Solid-State Sensors, Actuators and Microsystems, Lyon, France, 10-14 June 2007, pp. 1761-1764.

[27] E.A. Olson, M.Y. Efremov, A.T. Kwan, S. Lai, V. Petrova, F. Schiettekatte, F. Shiettekatte, J.T. Warren, M. Zhang, L.H. Allen, Scanning calorimeter for nanoliter-scale liquid samples, Applied Physics Letters, 77 (2000) 2671-2673.

[28] Y. Seung-Il, L. Mi-Hwa, P. Se-Chul, S. Jeon-Soo, K. Yong-Jun, Detection of Neisseria meningitidis using a micromachined split-flow microcalorimeter, in: Proceedings of the MEMS IEEE 20th International Conference on Micro Electro Mechanical Systems, Hyogo, Japan, 21-25 January 2007, pp. 509-512.

[29] Y. Seung-Il, L. Mi-Hwa, P. Se-Chul, S. Jeon-Soo, K. Yong-Jun, Neisseria meningitidis - detection based on a microcalorimetric biosensor with a split-flow microchannel, Journal of Microelectromechanical Systems, 17 (2008) 590-598.

[30] F. De Santis, S. Adamovsky, G. Titomanlio, C. Schick, Scanning nanocalorimetry at high cooling rate of isotactic polypropylene, Macromolecules, 39 (2006) 2562-2567.

[31] F. De Santis, S. Adamovsky, G. Titomanlio, C. Schick, Isothermal nanocalorimetry of isotactic polypropylene, Macromolecules, 40 (2007) 9026-9031.

[32] V. Guidi, M.A. Butturi, M.C. Carotta, B. Cavicchi, M. Ferroni, C. Malagù, G. Martinelli, D. Vincenzi, M. Sacerdoti, M. Zen, Gas sensing through thick film technology, Sensors and Actuators B: Chemical, 84 (2002) 72-77.

[33] R.E. Cavicchi, G.E. Poirier, N.H. Tea, M. Afridi, D. Berning, A. Hefner, J. Suehle, M. Gaitan, S. Semancik, C. Montgomery, Micro-differential scanning calorimeter for combustible gas sensing, Sensors and Actuators B: Chemical, 97 (2004) 22-30.

[34] A. Minakov, J. Morikawa, T. Hashimoto, H. Huth, C. Schick, Temperature distribution in a thin-film chip utilized for advanced nanocalorimetry, Measurement Science and Technology, 17 (2006) 199-207.

[35] Xensor-Integration, Standard products, in: http://www.xensor.nl/, 2010.

[36] H. Schubert, A. Kuznetsov, Peroxide explosives, in: H. Schubert, A. Kuznetsov (Eds.) the NATO Advanced Research Workshop, Springer, St. Petersburg, 2005, pp. 239.

[37] Y.-S. Liu, V.M. Ugaz, W.J. Rogers, M. Sam Mannan, S.R. Saraf, Development of an advanced nanocalorimetry system for material characterization, Journal of Loss Prevention in the Process Industries, 18 (2005) 139-144.

[38] W.W. Bannister, C.-C. Chen, W.A. Curby, E.B. Chen, P.L. Damour, A. Morales, Thermal Analysis for Detection and Identification of Explosives and Other Controlled Substances, in: U.S. Patent (Ed.) PatentStorm, University of Massachusetts, Boston, 2002.

[39] N. Piazzon, M. Rosenthal, A. Bondar, D. Spitzer, D.A. Ivanov, Characterization of explosives traces by the Nanocalorimetry, Journal of Physics and Chemistry of Solids, 71 (2010) 114-118.

[40] A. Zuck, J. Greenblatt, A. Zifman, A. Zaltsman, S. Kendler, G. Frishman, S. Meltzer, I. Fisher, Explosive detection by microthermal analysis, Journal of Energetic Materials, 26 (2008) 163 - 180.

[41] R.J. Graybush, F.G. May, A.C. Forsyth, Differential thermal analysis of primary explosives, Thermochimica Acta, 2 (1971) 153-162.

[42] V.H. Carreto-Vazquez, A.K. Wójcik, Y.-S. Liu, D.B. Bukur, M.S. Mannan, Miniaturized calorimeter for thermal screening of energetic materials, Microelectronics Journal, In Press, Accepted Manuscript (2010).

[43] R. Schulte-Ladbeck, P. Kolla, U. Karst, A field test for the detection of peroxide-based explosives, Analyst, 127 (2002) 1152-1154.

[44] S. Parajuli, W. Miao, Sensitive determination of hexamethylene triperoxide diamine explosives, using electrogenerated chemiluminescence enhanced by silver nitrate, Analytical Chemistry, 81 (2009) 5267-5272.

[45] V. Gaia, Explosives linked to London bombings identified, in: Electronic Newspaper, New Scientist, http://www.newscientist.com/article/dn7682, London, UK, 2005.

[46] R. Meyer, J. Kohler, A. Homburg, Explosives, Fifth ed., Wiley-VCH Verlag GmbH & Co. KGaA, Weinheim, Germany, 2002.

[47] J. Yinon, S. Zitrin, Modern Methods and Applications in Analysis of Explosives, John Wiley & Sons, Chichester, England, 1993.

[48] N.D. Tuyen, M. Evangelisti, A. Di Bona, M. Affronte, Membrane-based microcalorimetry for thin films and sub-milligram single-crystal, Journal of Physics: Conference Series, 187 (2009) 012034.

[49] E.A. Olson, M.Y. Efremov, Z. Ming, Z. Zishu, L.H. Allen, The design and operation of a MEMS differential scanning nanocalorimeter for high-speed heat capacity measurements of ultrathin films, Journal of Microelectromechanical Systems, 12 (2003) 355-364.

[50] A. Elshabini-Riad, F.D. Barlow, Thin-Film Technology Handbook, McGraw-Hill, New York, 1998.

[51] R. Ralph, Thermal Design of Electronic Equipmement, CRC Press LLC, Boca Raton, Florida, 2001.

[52] M. Imran, A. Bhattacharyya, Effect of thin film thickenesses and materials on the response of RTDs and microthermocouples, IEEE Sensors Journal, 6 (2006) 1459-1467.

[53] V.H. Carreto-Vazquez, Y.-S. Liu, D.B. Bukur, M.S. Mannan, Chip-Scale Calorimeters: Potential uses in chemical engineering, Journal of Loss Prevention in the Process Industries, In Press, Accepted Manuscript.

[54] R. Wüthrich, L.A. Hof, The gas film in spark assisted chemical engraving (SACE)--A key element for micro-machining applications, International Journal of Machine Tools and Manufacture, 46 (2006) 828-835.

[55] V. Fascio, H.H. Langen, H. Bleuler, C. Comninellis, Investigations of the spark assisted chemical engraving, Electrochemistry Communications, 5 (2003) 203-207.

[56] I. Mita, I. Imai, H. Kambe, Determination of heat of mixing and heat of vaporization with a differential scanning calorimeter, Thermochimica Acta, 2 (1971) 337-344.

[57] A.A. Minakov, S.A. Adamovsky, C. Schick, Non-adiabatic thin-film (chip) nanocalorimetry, Thermochimica Acta, 432 (2005) 177-185.

[58] COMSOL-Multiphysics, Reference Manual, 2009.

[59] N.I.M. Gould, Y. Hu, J.A. Scott, A numerical evaluation of sparse direct solvers for the solution of large sparse, symmetric linear systems of equations, in: Council for the Central Laboratory of the Research Councils, Oxfordshire, UK, 2005.

[60] H.-C. Huang, A.S. Usmani, Finite Element Analysis for Heat Transfer - Theory and Software, Springer-Verlag, London, U.K., 1994.

[61] A.F. Lopeandía, J. Rodríguez-Viejo, M. Chacón, M.T. Clavaguera-Mora, F.J. Muñoz, Heat transfer in symmetric U-shaped microreactors for thin film calorimetry, Journal of Micromechanics and Microengineering, 16 (2006) 965.

[62] A.G. Kozlov, Analytical modelling of temperature distribution in resistive thin-film thermal sensors, International Journal of Thermal Sciences, 45 (2006) 41-50.

[63] E. Zhuravlev, C. Schick, Fast scanning power compensated differential scanning nano-calorimeter: 1. The device, Thermochimica Acta, 505 (2010) 1-13.

APPENDIX

Modeling of Prototypes by Finite Element Analysis

This appendix is dedicated to describing the finite element models constructed to study the design of the chip-scale calorimeters used in this project. Information obtained from the models was used to estimate the temperature distributions, influence of boundary conditions, power consumption and electrical response of heaters and resistance temperature detectors.

Thin-film based calorimeters: Xensor TCG-3880 example

A thermal conductivity gauge TCG-3880 from Xensor Integration [35] was used as an example of nanocalorimeters based on thin-film silicon nitride technology. TCG-3880 gauges are not optimized for use in calorimetric applications [34]. However, because of their characteristics, TCG-3880 gauges have been used in ultra-fast nanocalorimetry in multiple research works [40, 57].

Device description

TCG-3880 gauges consist of a closed thin-film silicon nitride membrane of 50 x 100 μm^2 and 1 μm-thick. The membrane is supported by a silicon rim of 2.50 x 3.33 mm^2 and 300 μm-thick (Figure 23). The central area of the membrane is assumed to be isolated thermally from the surroundings due to the high thermal resistance achieved by its reduced thickness. Temperature monitoring in TCG-3880 gauge is done with a thermopile with an effective sensitivity of 1.3 mV/K. The thermopile hot junctions are placed around 50 μm

from the polysilicon heater, whereas the cold junction are placed at a distance of one millimeter. The heat required to operate the device is supplied by a 600 ohm polysilicon heater with a temperature coefficient of 0.1 %/^{o}C [35]. Additional specifications are given in Table 4.

Table 4 Specification parameters for TCG-3880 gauges (adapted from [35]).

Parameter	**TCG-3880**
Membrane thickness	1 μm
Hot spot area	50 x 100 μm^2
Overall Si frame dimensions	2.50 x 3.33 mm^2
Output in air	30 V/W
Thermopile resistance	55,000 ohm
Thermopile effective sensitivity (intrinsic)	1.3 (2.4) mV/K
Heater resistance	600 ohm
TCR	0.1 %/K
Thermal resistance in vacuum	100 kK/W
Maximum heating voltage in air (vacuum)	2.5 (1.0) V
Heater maximum temperature	250^{o}C

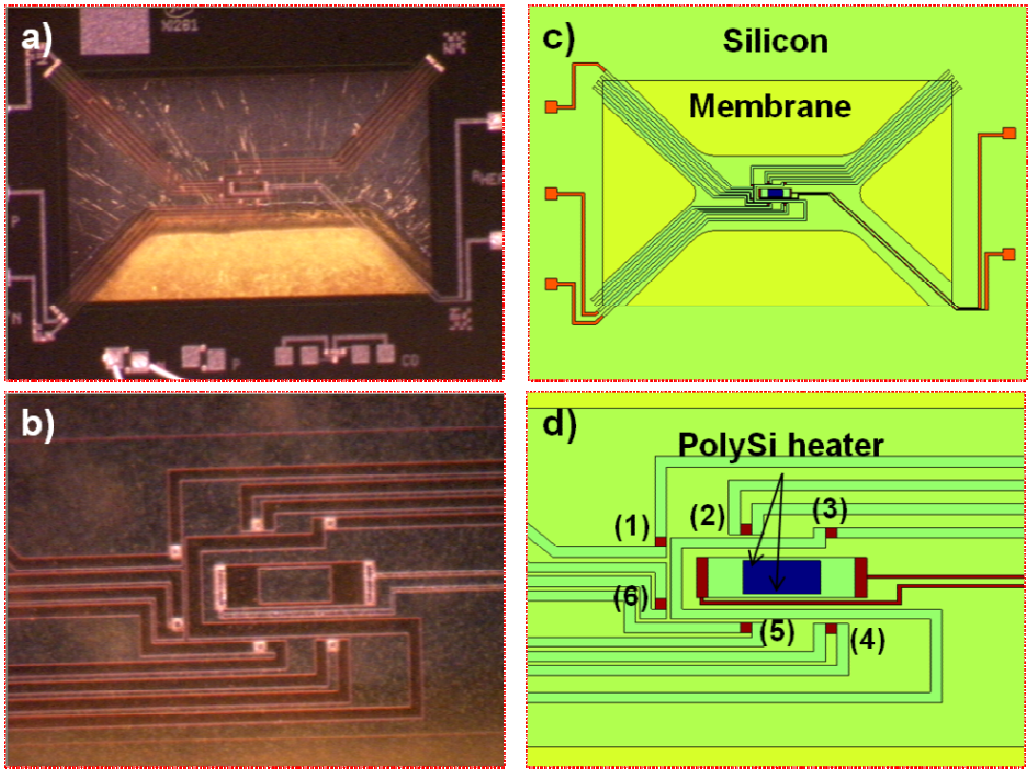

Figure 23 a) Picture of TCG-3880 gauge; b) magnification showing the thermopile leads and the polysilicon heater; c) and d) 2D model constructed with COMSOL Multiphysics™. Numbers indicate thermopile leads in the sensor.

Model construction – TCG-3880 gauge

A two-dimensional (2D) model of the TCG-3880 was constructed using the electro-thermal interaction module of COMSOL Multiphysics™. This module solves the equations that describe the electrical and heat transfer domains simultaneously. These equations are given as follows:

Electrical domain:

$$\boldsymbol{q_{Joule}} = \frac{\boldsymbol{I^2 \times R(T)}}{\boldsymbol{S_{Heater}}} \tag{A.1}$$

$$\boldsymbol{R(T)} = \boldsymbol{\delta(T)}\frac{\boldsymbol{L}}{\boldsymbol{A}} \tag{A.2}$$

$$\boldsymbol{\delta(T)} = \boldsymbol{\delta_o}\big(\mathbf{1} + \boldsymbol{\alpha(T - T_o)}\big) \tag{A.3}$$

where, I is the current flowing through the resistive heater (amps), $R(T)$ is the resistance of the heater as a function of temperature (ohms), S_{Heater} is the surface area of the heater (m^2), δ_o is the resistivity of the heater's material at the reference temperature (ohm-m), T_o is the reference temperature (K), α is the temperature coefficient of resistivity (K^{-1}), L is the length of the heater (m), and A is the cross sectional area of the heater (m^2).

Heat transfer domain:

$$\boldsymbol{\rho C_p \frac{\partial T}{\partial t} + \nabla \cdot (-k \nabla T) = Q - \rho C_p u \cdot \nabla T - E \cdot (T^4 - T_e^4)} \quad \text{(A.4)}$$

where ρ is the material density (kg/m^3), C_p is the specific heat capacity at constant pressure (J/kg-K), T is absolute temperature (K), $\boldsymbol{u}$ is the velocity vector (m/s), k is the thermal conductivity (W/m-K), Q represents heat sources other than viscous heating (W/m^3), E is the constant for thermal radiation and T_e is the external temperature (K).

The following sections describe the initial and boundary conditions used to solve these equations.

Electrical Domain - Boundary Conditions

The first boundary condition was fixed by assuming that the resistive heater is surrounded by isolating material and there are not current losses through the lateral walls of the heater, therefore:

$$\boldsymbol{n \cdot J = 0} \quad \text{(A.5)}$$

In a second boundary condition, an electrical potential between the terminals of the heaters of length *L* are established.

$$\boldsymbol{E}(\mathbf{0}, \boldsymbol{y}, \boldsymbol{z}) = \mathbf{0} \quad (\boldsymbol{ground}) \tag{A.6}$$

$$\boldsymbol{E}(\boldsymbol{L}, \boldsymbol{y}, \boldsymbol{z}) = \boldsymbol{V} \quad (\boldsymbol{applied\ voltage}) \tag{A.7}$$

where $\boldsymbol{J}$ is the input current density (amps/m^3) and V is the applied voltage (volts).

For the model construction, the geometric dimensions were approximated from microscope images of the sensor, and from personal communications with the manufacturer. Five sub-domains were created and their properties were assigned to match the properties of the construction material in the sensor. Then a triangular mesh of 31,811 elements was applied to the 2D model (see Figure 24a).

The 2D model was solved by finite element analysis using the a Direct (UMFPACK) [58-59] linear system solver method, which is included in COMSOL Multiphysics™. The current supplied to the heater was increased following the expression $I_{rate}/60*t^N$, where I_{rate} is the current rate, t is the time in seconds and N is a constant selected to simulate an approximate linear heating of the calorimeter. The results collected from the model include the electrical potential

across the heater, resistance change, and joule heating. Figure 24 show the electrical potential and the joule heating obtained when applying a current of 4.6 mA to the polysilicon heater. More detailed results will be discussed in a following section.

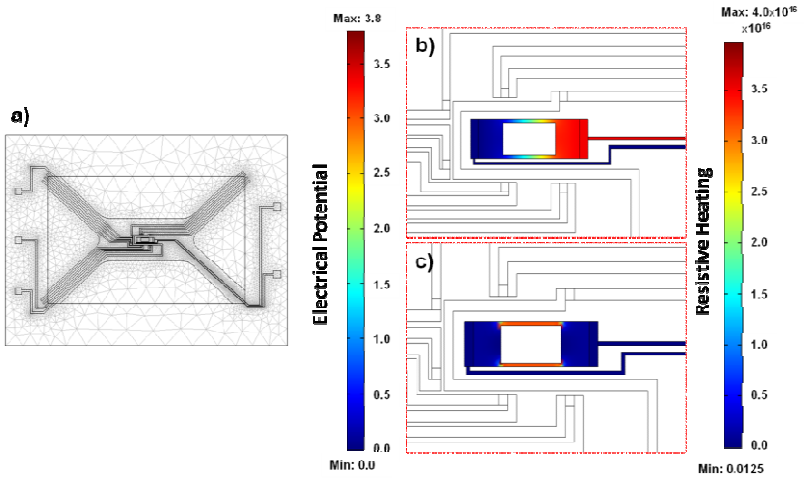

Figure 24 Postprocessing results obtained from TCG-3880 2D model in the electrical domain: a) meshed geometry, b) electrical potential distribution, c) resistive heating.

The power required to operate the TCG-3880 gauges is equal the electrical power produced in polysilicon heaters. The basic assumption is that all this electrical heat is transferred to the calorimeter/sample and it is used to increase their temperature. The modeling of this heat transfer was modeled as follows:

Heat transfer - Initial Conditions

The initial conditions used to solve the heat transfer equations were fixed assuming that the temperature of the TCG-3880 gauge in all points is homogeneous and it is in complete thermal equilibrium with the surrounding air. Therefore, its temperature at time zero is equal to the ambient temperature.

$$\boldsymbol{T\big(x, y, z, (t = 0)\big) = T_{amb}} \tag{A.8}$$

Heat transfer - Boundary Conditions

The first boundary condition specified the temperature on the edge of the TCG-3880 gauge (Dirichlet boundary condition). Here, the backside of the device was connected directly to the chip holder, which is massive in relation to the calorimeter itself. The temperature of the chip holder was assumed constant and equal to the ambient temperature at all times [60-61]. Also, the temperature at the edges of the membrane was assumed to be constant and equal to the ambient temperature (25 deg C). This should be a reasonable assumption, since the 300 μm-thick silicon frame has a much larger heat capacity than the membrane, and should not heat significantly.

$$\boldsymbol{T|_{Surface} = T_{amb}} \tag{A.9}$$

A second boundary condition can be stated on the lateral walls of the calorimeter. The total area of the lateral sides is considerably smaller in relation to the upper and lower faces of the calorimeter. Then, it is reasonable to assume that the heat flow through the lateral walls is negligible [62]. As a simplification these walls can be assumed as perfectly insulated, hence:

$$-\boldsymbol{n}|_{\boldsymbol{Surface}} \cdot \boldsymbol{q} = \boldsymbol{q_o} = \boldsymbol{0} \tag{A.10}$$

and

$$\boldsymbol{q} = -\boldsymbol{k}\boldsymbol{\nabla}\boldsymbol{T} + \boldsymbol{\rho}\boldsymbol{C_p}\boldsymbol{u}\boldsymbol{T} \tag{A.11}$$

where: q_o is the inward heat flux, which is normal to the boundary (W/m^2) and **n** is the normal vector of the lateral walls. On the other hand, the upper face of the calorimeter is exchanging heat with the surroundings. Therefore, this layer is defined by the following expression:

$$-\boldsymbol{n}|_{\boldsymbol{Surface}} \cdot (-\boldsymbol{k}\boldsymbol{\nabla}\boldsymbol{T}) = \boldsymbol{h}(\boldsymbol{T} - \boldsymbol{T_{amb}})|_{\boldsymbol{Surface}} \tag{A.12}$$

Finally, the heaters can be considered as a heat sources due to Joule effects (see previous section). The expression that represents them is:

$$-\boldsymbol{n}|_{\boldsymbol{Surface}} \cdot (-\boldsymbol{k}\boldsymbol{\nabla}\boldsymbol{T}) = \boldsymbol{q_{Joule}} + \boldsymbol{h}(\boldsymbol{T} - \boldsymbol{T_{amb}})|_{\boldsymbol{Surface}} \tag{A.13}$$

Additional assumptions are that the temperature gradients in the z-direction of the calorimeter are negligible. The thickness of the calorimeter is much smaller than the lateral dimensions, and hence this assumption is a reasonable simplification. Finally, the heat transfer equation can be simplified by assuming that the heat generated by the electrical heaters is transmitted to the calorimeter and the sample mainly by conduction mechanisms. Therefore, thermal radiation and convection were neglected.

Figure 25 shows 2D postprocessing results of the TCG-3880 gauge with the corresponding temperature profile obtained from simulations in the transient mode. The plots show a steady-state screen shot when there is a differential voltage of 3.8 volts across the polysilicon heater. For the model the effect of the temperature on the properties of the material was taken into account by coupling the electrical domain equations with the heat transfer domain equations. With this it was possible to predict the change in resistance at different temperatures and the changes in heat capacity of the calorimeter. Experimental results will be included in a subsequent section in order to test the validity of the COMSOL Multiphysics™ model.

As it can be seen from the 2D models, in TCG-3880 gauges the heated area is well insulated from the surroundings due to the good thermal insulation achieved by the reduced thickness of the membrane. However, the lateral temperature gradients are large due to the non-homogeneous heating. This is

because the heater consists of two resistive heater stripes confined to a small area in the center of the membrane. Figure 25 (b and d) shows temperature gradients of several degrees around the heaters in very short distances. This confirms that the sample should be precisely placed inside the heated area for accurate results. Similar findings have been reported by Zhuravlev and Schick [63] using other thin-membrane nanocalorimeters developed by Xensor Integration ($i.e.$, XI-292, XI-320, XI-296).

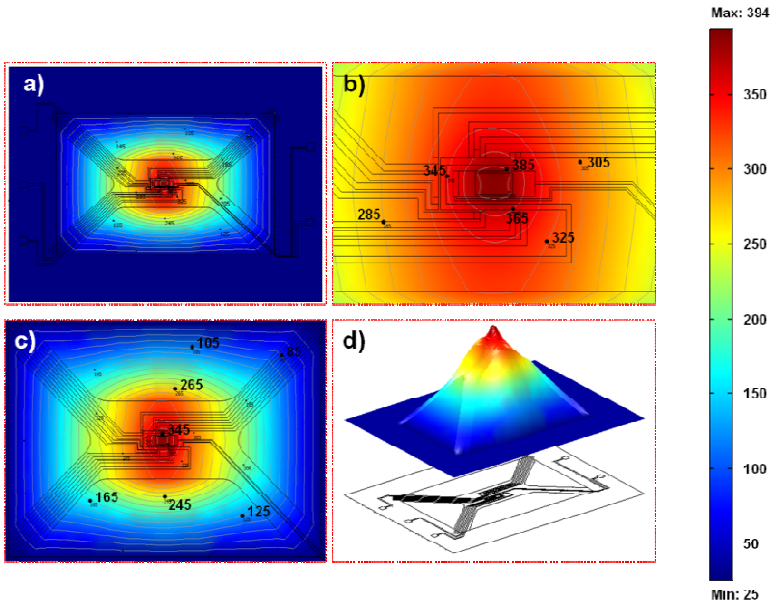

Figure 25 Postprocessing results showing the temperature distribution obtained from TCG-3880 2D model in the heat transfer domain.

Thick-membrane based calorimeters: Xensor NCM-9924

A different type of chip-scale calorimeters are based on thick silicon membranes. These devices are typically used with liquid samples because they are robust and the space behind the membrane can be used to contain the sample. However, due to their thicker membrane the thermal resistance is smaller compared to devices based on silicon nitride membranes. As an example of these devices we used a commercial NCM-9924 liquid nanocalorimeter from Xensor Integration [24, 35].

Device description

NCM-9924 devices have aluminum thin-film resistive heaters, which have a resistance of 260 or 1050 ohms depending on the electrical connections (see Figure 26). Also these sensors have an additional p-type silicon resistor of 440 ohms. The heater design and the excellent thermal conductivity of silicon allow a relatively homogeneous temperature distribution over the entire membrane. However, because of its lower thermal resistance compared to thin-film based calorimeters, heat losses by lateral conduction through the chip carrier are expected especially at high temperatures, which reduce their sensitivity and increase the power requirements to operate these devices. These calorimeters have a limited temperature range of operation (~100^{o}C) because the electrical behavior of the materials used in their fabrication changes. Additional specifications for NCM-9924 liquid calorimeters are given in Table 5

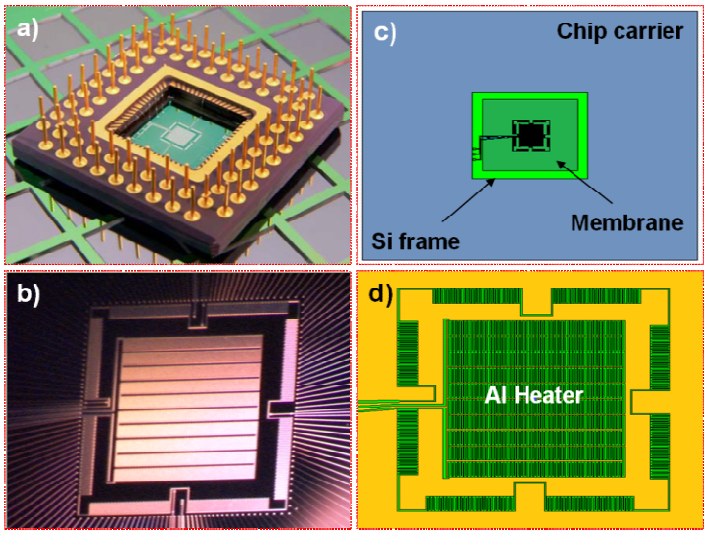

Figure 26 a) Picture of NCM-9924 liquid calorimeter; b) magnification showing the thermopile leads and the Al heater; c) and d) 2D model constructed with COMSOL Multiphysics™.

Table 5 NCM-9924 nanocalorimeter specifications (adapted from [35]).

Parameter	NCM-9924
Membrane thickness	22-45 μm
Membrane area	8.3×8.3 mm^2
Overall Si frame dimensions	10.0×10.0 mm^2
Output in air	1.2-2.4 V/W
Output in water	---
Thermopile resistance	50,000 ohm
Thermopile sensitivity (intrinsic)	50 mV/K
Heater resistance	440 (800, 260) ohm
Thermal resistance	24-48 K/W

Model construction: NCM-9924 liquid nanocalorimeter

NCM-9924 liquid nanocalorimeters 2D models were also modeled constructed using the electro-thermal interaction module of COMSOL Multiphysics™. Here, the chip carrier also modeled because its heat transfer with the nanocalorimeter cannot be neglected.

Heat transfer - Initial Conditions

In a similar way that for TCG-3880 gauges, the initial conditions used to solve the heat transfer equations were fixed assuming that the temperature of the NCM-9924 liquid nanocalorimeter is homogeneous in all points and it is equal to the ambient temperature (eq. A.8).

Heat transfer - Boundary Conditions

A Dirichlet boundary condition was chosen to solve the 2D model for the NCM-9924 liquid nanocalorimeter. Here, the temperature on the edge of the chip carrier was initially set to be equal to the ambient temperature (25^{o}C). The interior boundaries of the model ($i.e.$, frontier between chip carrier and liquid calorimeter) were assumed to freely exchange heat by conduction mechanisms. This condition represents the heat dissipation that occurs from the heated area of the device to the chip carrier and its surroundings.

The final boundary condition exists between the thin film heater and the surface of the membrane. Here, the heat flux through the boundary is specified and it is equal to the joule heating per unit area (eq. A.10).

Figure 27 shows 2D postprocessing results of the NCM-9924. As it can be observed from these results, the heated area is not completely insulated and the chip carrier will heat due to conduction mechanisms. On the other hand, the lateral temperature gradients in NCM-9924 sensors are smaller due to the excellent thermal conductivity of silicon. This has the limitation that the sensitivity of the device will be affected. On the other hand, Figure 28 shows the temperature distribution of the calorimeter device at different positions as a function of the applied voltage. As it can be observed the voltage required by this device is larger compared to TCG-3880 gauges because the larger mass of the sensor. This is a disadvantage in terms of device sensitivity, but this problem is compensated for the robustness of NCM-9924 sensor, which can be used in applications with liquid samples and without requiring special handling of the sample under analysis.

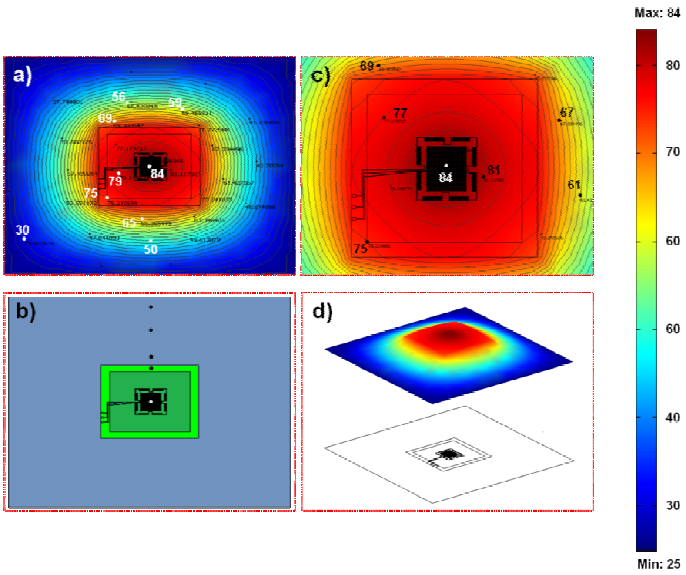

Figure 27 Postprocessing results showing the temperature distribution obtained from NCM-9924 2D model.

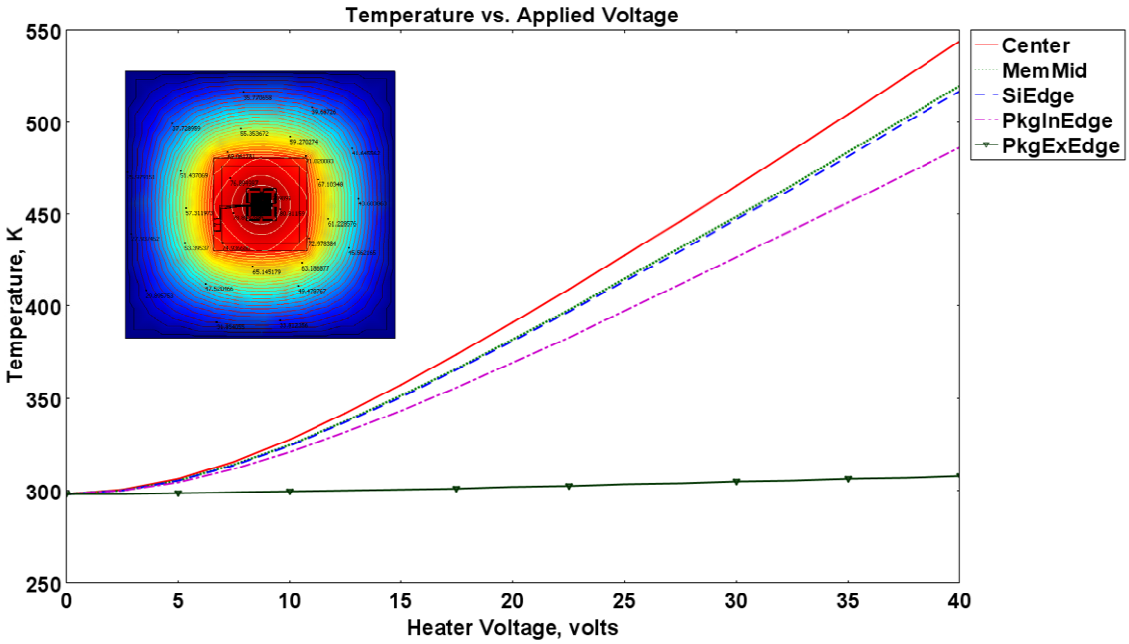

Figure 28 Temperature profile for calorimeter NCM-9924 obtained from 2D FEA models as a function of the applied voltage to de heaters.

VITA

Victor Hugo Carreto Vazquez received his Bachelor of Science degree in Industrial Chemical Engineering from the National Polytechnic Institute (IPN) at Mexico City in 1999. He joined the IPN as a young assistant professor in January 2000 and was promoted to associate professor in 2003. He entered the Chemical Engineering program at Texas A&M University in January 2001 and received his Master of Science degree in August 2003. In 2004 he joined Celanese Mexicana from 2004 to 2005 working as a production engineer leader. His research interests include reactive chemicals, dust explosions and static electricity. He plans to continue his professional career in the area of process safety.

Mr. Carreto Vazquez may be reached at Gardenia # 206, Col. Las Flores, Cd. Netzahualcóyotl, Estado de México, México, 57310. Mr. Carreto's personal email address is kbas_57310@hotmail.com.